Analytica Chimica Acta 825 (2014) 1–25

Contents lists available at ScienceDirect

Analytica Chimica Acta

journal homepage: www.elsevier.com/locate/aca

Review

Silicon nanowires as field-effect transducers for biosensor development: A review

M. Omair Noor, Ulrich J. Krull *

Chemical Sensors Group, Department of Chemical and Physical Sciences, University of Toronto Mississauga, 3359 Mississauga Road North, Mississauga, ON L5L 1C6, Canada

HIGHLIGHTS

- Nanoscale field-effect transducers interrogate surface charge by conductivity changes.
- The nanometer dimensions of SiNWs facilitate sensitive detection of biomolecules.
- SiNWs can be fabricated by bottom–up or top–down approaches.
- Device parameters and solution-phase conditions strongly influence analytical performance.

GRAPHICAL ABSTRACT

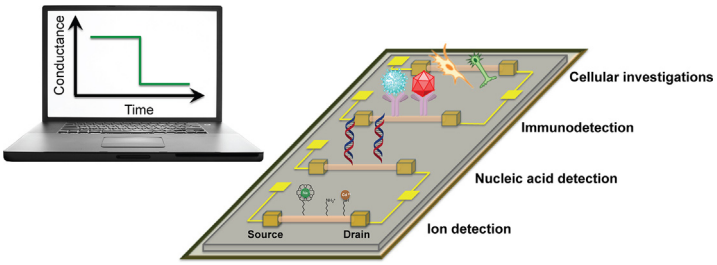

ARTICLE INFO

Article history:
Received 31 December 2013
Received in revised form 11 March 2014
Accepted 13 March 2014
Available online 15 March 2014

Keywords:
Silicon nanowires
Field effect transistors
Surface functionalization

ABSTRACT

The unique electronic properties and miniaturized dimensions of silicon nanowires (SiNWs) are attractive for label-free, real-time and sensitive detection of biomolecules. Sensors based on SiNWs operate as field effect transistors (FETs) and can be fabricated either by top–down or bottom–up approaches. Advances in fabrication methods have allowed for the control of physicochemical and electronic properties of SiNWs, providing opportunity for interfacing of SiNW-FET probes with intracellular environments. The Debye screening length is an important consideration that determines the performance and detection limits of SiNW-FET sensors, especially at physiologically relevant conditions of ionic strength (>100 mM). In this review, we discuss the construction and application of SiNW-FET sensors for detection of ions, nucleic acids and protein markers. Advantages and disadvantages of the top–down and bottom–up approaches for synthesis of SiNWs are discussed. An overview of various

Abbreviations: 1 BPM, 1 base pair mismatch; 1-D, 1-dimensional; 2-MEA, 2-mercaptoethylamine; 3-D, 3-dimensional; Act-D, actinomycin-D; Ad, adamantane; AIV, avian influenza virus; AMPs, antibody mimic proteins; anti-cTnI, antibody for cTnI; anti-hIgG, antibody for human IgG; APTES, 3-aminopropyltriethoxysilane; ASIC, application specific integrated circuit; β-CD, β-cyclodextrin; BB, blown–bubble; BG, back-gate; BIT-FET, branched intracellular nanotube FET; BP, base pair; BSA, bovine serum albumin; CaM, calmodulin; CEA, carcinoembryonic antigen; CK-MB, creatine kinase MB; CK-MM, creatine kinase MM; CMOS, complementary metal oxide semiconductor; cTnI, cardiac Troponin I; cTnT, cardiac Troponin T; CVD, chemical vapor deposition; D, drain; DG, double-gate; DMPC, 1,2-dimyristoyl-sn-glycero-3-phosphocholine; DNA, deoxyribonucleic acid; DTT, dithiothreitol; ECG, electrocardiogram; EDTA, ethylenediaminotetraacetic acid; ELISA, enzyme-linked immunosorbent assay; FC, fully-complementary; FET, Field effect transistor; FG, front-gate; G, gate; GSH, glutathione; GST, glutathione S-transferase; H-terminated, hydrogen terminated; hIgG, human IgG; His-tag, histidine tag; I_{sd}, source–drain current; LB, Langmuir–Blodgett; LOD, limit of detection; mAb, monoclonal antibody; mES, mouse embryonic stem; MPTES, 3-mercaptopropyltriethoxysilane; MPTMS, 3-mercaptopropyltrimethoxysilane; NC, non-complementary; NTA, nitrilotriacetic acid; NW, nanowire; PBS, phosphate buffered saline; PDMS, polydimethylsiloxane; PNA, peptide nucleic acid; PSA, prostate specific antigen; PSAα1, PSA-α1-antichymotrypsin; RCA, rolling circle amplification; RE, reference electrode; S, source; SEM, scanning electron microscope; SiNW, Silicon nanowire; siRNA, small interfering RNA; SNP, single nucleotide polymorphism; SOI, silicon-on-insulator; SSC, saline sodium citrate; ssDNA, single-stranded DNA; TCEP, *tris*(2-carboxyethyl) phosphine; TEM, transmission electron microscope; TNF-α, tumor necrosis factor-alpha; TUNEL, terminal deoxynucleotidyl transferase dUTP nick end labeling; V_{bg}, back-gate voltage; V_G, gate voltage; V_{lg}, liquid gate voltage; V_{sd}, source–drain voltage; VLS, vapor–liquid–solid.

* Corresponding author. Tel. +1 905 828 5437; fax: +1 905 828 5425.
E-mail address: ulrich.krull@utoronto.ca (U. J. Krull).

http://dx.doi.org/10.1016/j.aca.2014.03.016
0003-2670/

Gating
Debye length

methods for surface functionalization of SiNWs for immobilization of selective chemistry is provided in the context of impact on the analytical performance of SiNW-FET sensors. In addition to *in vitro* examples, an overview of the progress of use of SiNW-FET sensors for *ex vivo* studies is also presented. This review concludes with a discussion of the future prospects of SiNW-FET sensors.

Contents

1. Introduction . . . 2
2. Silicon nanowires: device preparation, alignment methods, surface functionalization and effects of nanowire properties on assay performance 3
2.1. SiNWs as field-effect transistors . . . 3
2.2. SiNW-FETs fabrication . . . 4
2.2.1. Synthesis of SiNWs via vapor–liquid–solid mechanism . . . 4
2.3. Alignment of SiNWs . . . 5
2.3.1. Langmuir–Blodgett alignment . . . 6
2.3.2. Blown–bubble alignment . . . 6
2.3.3. Microfluidic flow alignment . . . 6
2.3.4. Electric-field alignment . . . 7
2.3.5. Contact printing alignment . . . 8
2.4. Surface functionalization . . . 9
2.4.1. Reusable interfacial chemistries . . . 12
2.5. Charge screening and Debye length . . . 13
2.6. Effects of NW diameter, number and doping density on assay performance . . . 13
3. Applications . . . 14
3.1. SiNWs as ion selective nanosensors . . . 14
3.2. Nucleic acid detection using SiNWs . . . 15
3.3. Immunodetection using SiNWs . . . 18
3.3.1. Multiplexed detection . . . 20
3.4. Cellular investigations using SiNW-FET probes . . . 21
3.4.1. Intracellular delivery of agents . . . 23
4. Summary and conclusions . . . 23
Acknowledgements . . . 23
References . . . 23

Omair Noor received his Hon. B.Sc. degree in Biotechnology specialist program, in 2008, and M. Sc. degree in Bio-Analytical Chemistry, in 2010, from the University of Toronto Mississauga, Mississauga, ON, Canada. He is currently working towards his Ph. D. degree in the department of Chemistry at University of Toronto with the Chemical Sensors Group under the supervision of Prof. Ulrich J. Krull. His research interests focus on the integration of quantum dots and FRET based assays for nucleic acid detection using microfluidic channels and paper as a solid support. Omair currently holds an Ontario Graduate Scholarship (OGS) from the Ontario Ministry of Training, Colleges and Universities (MTCU). He was also a recipient of Undergraduate Student Research Award (USRA) from the Natural Sciences and Engineering Research Council of Canada (NSERC).

Ulrich Krull is appointed as a Professor of Analytical Chemistry at the University of Toronto, and holds the endowed AstraZeneca Chair in Biotechnology. His research interests are in the areas of biosensor and diagnostic technologies, and applications to biotechnology, forensic, clinical and environmental chemistry. His research work is exploring the use of luminescent nanoscale materials and microfluidics technologies to build devices for detection of DNA and RNA targets. Krull is an editor for Analytica Chimica Acta, and serves on a number of Scientific Advisory Boards for industry.

1. Introduction

The integration of nanomaterials into device structures for biosensing applications has played a central role in the development of new strategies for signal transduction [1,2]. Due to comparable sizes of biological macromolecules and nanomaterials (nanotubes, nanowires and nanoparticles), the combination of nanomaterials with biomolecules offers potential for development of sensing technologies of molecular size scale for sensitive detection of biomolecules [2]. Silicon nanowires (SiNWs) are a class of 1-dimensional (1-D) nanomaterial that was introduced in 2001 by the Lieber group [3]. Since this time SiNWs have been described in numerous studies as electrical field-based sensors that are suitable for a variety of applications that include detection of ions [4,5], small molecules [6,7], nucleic acids [8], proteins [9] and the investigation of the electrophysiology associated with single cells [10–13] and tissues [14,15]. SiNWs can be synthesized as single crystals, and owing to their 1-D morphology and resulting increase in surface area-to-volume ratio, they provide improved analytical sensitivity as compared to planar field effect transistor (FET) devices for chemical and biosensing [16,17]. Advances in synthetic approaches for fabrication of SiNWs have allowed for the control of morphology and doping levels of SiNWs [18], enabling SiNW-FETs for cellular studies with high spatial and temporal resolution [19]. Additionally, SiNWs offer label-free, real-time and ultrasensitive detection of biomolecules to sub-fM detection limits [20]. These detection limits are 2–3 orders of magnitude lower than those that have been reported with quantum dots and carbon nanotubes for ensemble compatible measurements [1]. Top–down fabrication of sensors based on silicon nanostructures offers the practical advantage of compatibility with the established fabrication

processes of silicon-based complementary metal oxide semiconductor (CMOS) technology [21].

One of the main challenges associated with SiNW-FET sensors is the sensitivity to the ionic strength of a solution, where high ionic strength has detrimental effects on sensitivity. As a result, the detection of low quantities of protein and nucleic acid markers under physiological conditions of ionic strength has been reported to be a challenge [22]. This review will describe the construction and evaluation of SiNWs as biosensors, and will highlight efforts that have been made to address the issue of sensitivity to ionic strength. Some of the challenges associated with the development of SiNW-FET devices for large scale multiplexing capability will also be discussed. Additionally, recent developments in which SiNW-FETs are used for cellular recording and intracellular interfacing will be presented.

2. Silicon nanowires: device preparation, alignment methods, surface functionalization and effects of nanowire properties on assay performance

2.1. SiNWs as field-effect transistors

Field-effect devices measure charge at an interface, operating on the basis of two orthogonal circuits as shown in Fig. 1a [23]. The device takes the form of a n-p-n or p-n-p transistor, where n and p refer to n-doped and p-doped semiconductor, respectively. One circuit capacitatively connects a substrate (the sandwiched semiconductor; p-type Si in Fig. 1a) to a reference electrode (RE) and is responsible for applying a gate voltage (V_G) across a dielectric interface to adjust the potential at an interface that is in contact with a sample solution [23]. In another circuit, a voltage (V_{sd}) is applied across the channel region between the source and a drain to allow a current flow (I_{sd}) from the source to the drain. The density of charge carriers in the channel region of the substrate is modulated by the gate voltage, which in turn affects the threshold voltage that is required for device operation [24]. In the case of a p-type substrate, an application of positive gate voltage across the dielectric interface leads to a depletion of charge carriers in the channel region resulting in a decrease in conductivity (Fig. 1b(i)), while an application of negative gate voltage leads to an accumulation of charge carriers in the channel region resulting in an increase in conductivity (Fig. 1b(ii)) [25].

FETs can be configured as transducers for chemical and biological sensors by modifying the dielectric interface with a selective chemistry. Upon analyte binding, e.g., single-stranded DNA (ssDNA) binding with a complementary probe immobilized at the interface, the surface charge introduced at the interface is analogous to applying a new gate voltage across the interface, which in turn influences the density of charge carriers in the channel region, and hence conductivity. Overall, FETs respond by conductivity changes that are caused by variations in the electric field across the dielectric interface.

SiNWs are 1-D nanomaterials with a single crystalline silicon core that is covered with an amorphous sheath of silicon oxide [26,27]. These NWs can exhibit either n-type or p-type conductivity with a cross-sectional diameter that can range from two to hundreds of nanometers and length in micrometers [28]. In terms of FET performance, SiNWs exhibit greater sensitivity than planar FET devices owing to reduced dimensionality and large surface area-to-volume ratio. The nanometer thickness of 1-D SiNWs and 2-D silicon nanoribbons renders the conduction channel depth to be in close proximity to the surface (within the size scale of the Debye screening length) [29,30]. As a result, a binding interaction causes charge accumulation or depletion in the entire cross-section of the wire as compared to only a thin region near the surface of much larger planar FET devices [25]. This unique feature of SiNWs provides sufficient sensitivity to enable detection of charge changes that are induced by the presence of single molecules and viruses at the gate [17].

A number of different sensor configurations have been reported in the literature. The choice of configuration affects the sensitivity

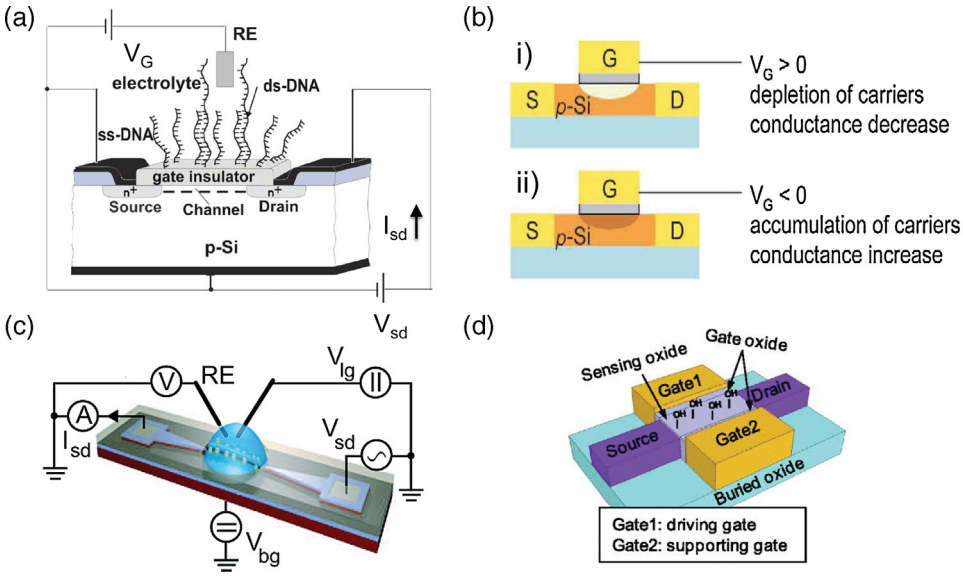

Fig. 1. (a) Schematic of a planar FET sensor for transduction of nucleic acid hybridization. (b) Schematics depicting changes in the density of charge carriers in the channel region for a p-type FET device under (i) a positive gate voltage and (ii) a negative gate voltage. (c) Schematic of a dual-gated FET sensor with the back-gate voltage applied through the silicon substrate and the front-gate voltage (also referred to as liquid gate voltage) applied via a platinum electrode that is placed in contact with the solution. The reference electrode (RE) is also placed in contact with the solution to measure the solution potential. (d) Schematic of a double-gate FET sensor with the two gates (gate 1 and gate 2) straddling both sides of the NW sensor. Panel (a) reprinted with permission from reference [23], panel (b) reprinted with permission from reference [25], panel (c) reprinted with permission from reference [31] and panel (d) reprinted with permission from reference [24].
Abbreviations: V_{sd}, source–drain voltage; RE, reference electrode; I_{sd}, source–drain current; V_{bg}, back-gate voltage; G, gate; S, source; D, drain; V_G, gate voltage; V_{lg}, liquid gate voltage.

of the device, and designs include back-gate (BG), front-gate (FG) and a double-gate (DG) structures [31]. The gating is done to modulate the density of charge carriers in the channel region [32,33]. In the case of a BG configuration, a voltage is applied via a back electrode that is placed underneath the channel region. In case of a FG configuration, a voltage is applied via an electrode that is placed in contact with the surrounding analyte solution. The FG and BG structures can be operated concurrently as a multigate device structure as shown in Fig. 1c, which is also referred to as dual-gated FET sensors [31,34,35]. The DG configuration consists of primary (driving) and secondary (supportive) gates, where the two gates vertically flank both sides of a NW as shown in Fig. 1d [24,36]. The conventional BG configuration suffers from a number of limitations in comparison with the DG configuration. Firstly, an application of bias voltage at the supportive gate lowers the threshold voltage and sub-threshold slope; it is the shift in the threshold voltage upon analyte binding which serves as a sensing metric [36]. Secondly, the BG configuration serves as a "global" gate and excludes the possibility of addressing the NW sensors individually. Alternatively, the DG configuration allows for independent control of the voltages at each of the two gates. This facilitates precise control of the channel potential, i.e., the conduction path of charge carriers in the channel region [24]. The result is control of device sensitivity by virtue of improvement in sub-threshold slope, greater shift in the threshold voltage and source–drain current upon analyte binding, provided that the voltage bias applied at the secondary gate is greater than the threshold voltage [36]. As an example, Ahn et al. reported a pH response of 68 mV pH^{-1} at 300 K from a DG NW-FET pH sensor when operating in an asymmetric mode [24]. It should be noted that the theoretical upper limit of shift in the threshold voltage for a conventional back gate NW-FET pH sensor is 59 mV pH^{-1} at 300 K, as predicted by the Nernst equation [31].

2.2. SiNW-FETs fabrication

The two approaches to fabricate SiNW-FET devices are classified as being top–down and bottom–up [37,38]. In a top–down approach, the fabrication methods of microelectronics industry are used to reduce the dimensionality of a bulk silicon wafer to generate SiNW-FETs. These methods include patterning, photolithography, reactive ion etching, ion-implantation, and e-beam lithography etc. The details of the top–down approaches for fabrication of SiNW-FETs have been discussed elsewhere [21,39–42] and will not be reviewed herein. In a bottom–up approach, the NWs are first synthesized, typically via chemical vapor deposition (CVD) reaction, prior to their assembly on a device substrate and fabrication of electrodes for electrical contacts by means of photolithography or e-beam lithography [38]. In terms of the bottom–up approach, the vapor–liquid–solid (VLS) growth method is a commonly used method for fabrication of SiNWs [27] and will be discussed in some detail. A greater in-depth discussion about the bottom–up synthesis of NWs can be found elsewhere [28,43–47]. Table 1 provides a comparison of the two fabrication approaches, including advantages and disadvantages associated with each fabrication approach.

2.2.1. Synthesis of SiNWs via vapor–liquid–solid mechanism

In terms of the bottom–up approach, the vapor–liquid–solid (VLS) growth method for fabrication of NWs is attractive as it results in a generation of single crystalline SiNWs [25]. This method uses a metal catalyst as an impurity to promote 1-D and anisotropic synthesis of SiNWs [28]. The metal catalyst is chosen such that it can form a liquid alloy with the NW material of interest (e.g., Si). The choice of synthesis temperature and target material (catalyst:nanowire material) composition is based on a phase diagram such that there is a coexisting metal catalyst and nanowire

Table 1
Comparison of the top–down and bottom–up approaches for synthesis of SiNWs.

	Top–down approach	Bottom–up approach
Device preparation	• SiNWs and device fabrication are done by etching a bulk silicon wafer (e.g., silicon-on-insulator (SOI) wafer). • Fabrication techniques are derived from CMOS technology. E.g., optical lithography, oxidation, reactive ion etching, deposition, ion-implantation, e-beam lithography, anisotropic wet etching etc. [48]. • For a scanning electron microscope (SEM) image, see Fig. 2c.	• SiNWs are synthesized from molecular precursors using a metal nanocluster mediated VLS mechanism, prior to assembly and integration of NWs with the circuitry for device fabrication [49–51]. • For a transmission electron microscope (TEM) image, see Fig. 2b.
Advantages	• Amenable to mass production. • Reliability and reproducibility of the fabrication process. • No integration issues, i.e., precise alignment and positioning of a specific number of NWs bridging the source and drain electrodes can be achieved. • NWs with different cross sections, such as triangular [52,53] and trapezoidal [21], can be fabricated (important for selective functionalization of NWs [52] and surface packing density of chemistry [54,55]). • NWs with double-gate structures that are supported on a co-planar geometry can be fabricated (improved sensitivity) [24,36].	• Flexibility of choice of material for NW fabrication. • Different doping levels and choice of dopants can be introduced during the synthesis (advantageous for dynamic range tuning). • Synthesis of SiNWs with diameter less than 10 nm is possible [56] (improved analytical sensitivity [57]). • Suitable for developing multilayer NW device structures (e.g., 3-D multilayer electronics) [58]. • Orientation and directional control of the growth of NW crystal is possible (e.g., kinked NWs and p-n junction NWs for intracellular interfacing) [11,18]. • Amenable to integration with flexible and transparent device substrates [14].
Disadvantages	• Time-consuming (serial fabrication process). • Expensive. • Limited choice of materials for NW fabrication. • Incompatibility of surface chemistry with the harsh treatments of nanofabrication. • Dimensions of NWs limited by the resolution of the fabrication process (NW diameter = 20–100 nm).	• Results in distribution of lengths and dimensions of the synthesized SiNWs. • Device fabrication requires precise alignment and positioning of SiNWs leading to integration issues. • Difficult to achieve precise control of number of SiNWs bridging the source and drain electrodes leading to variations in batch-to-batch fabrication of SiNW devices. • Alignment issues associated with long NWs (NWs with length in hundreds of micrometers) [59]. • Limited in terms of mass production of SiNW devices.

material as an alloy in liquid phase and solid nanowire material. The liquid catalyst serves as a preferential absorption site for gas-phase reactant (e.g., silane, SiH_4, in case of synthesis of SiNWs) [60]. Once this liquid catalyst cluster becomes supersaturated, it serves as a nucleation site for crystallization by promoting 1-D growth of NW material of interest in the presence of gas-phase reactants, provided that the catalyst cluster remains in liquid phase [60]. The size of the liquid catalyst cluster determines the diameter of SiNWs [28,56]. In addition, the growth axis of a SiNW is a function of the diameter of a SiNW [50]. Moreover, a directional control of the growth of a SiNWs during the synthesis process can be achieved *in situ* by controlling the partial pressure of gas phase reactants (e.g., kinked or zigzag SiNWs) [18].

A method combining laser ablation mediated catalyst cluster formation and VLS growth for synthesis of SiNWs was reported by Morale and Lieber [51]. The generation of catalyst clusters using laser ablation to set the minimum NW diameter (size 2–3 nm) is advantageous as it overcomes the size limitations of cluster formation using equilibrium cluster formation (size >200 nm) [28]. Consider a synthesis of SiNWs using a phase diagram shown in Fig. 2a(i). It can be seen that above 1200 °C, there is a broad area in the Si-rich region of the phase diagram where the liquid alloy of $Si_xFe_{1-x(l)}$ and solid $Si_{(s)}$ coexist. Hence, under the aforementioned temperature conditions and with the use of binary $Si_{0.9}Fe_{0.1}$ as a target material, it is possible to synthesize SiNWs. The apparatus used to synthesize SiNWs using VLS growth method and laser ablation to drive the formation of nm-sized catalyst clusters is shown in Fig. 2a(ii). The growth mechanism of SiNWs using this approach is shown in Fig. 2a(iii). Laser ablation of the $Si_{0.9}Fe_{0.1}$ target material produces a hot vapor of Si and Fe species that condenses into liquid clusters upon collision with the buffer gas. The temperature of the furnace is maintained above 1200 °C such that the condensed clusters remain in liquid phase. The growth of SiNW begins as the cluster becomes supersaturated with Si and this growth continues as long as the cluster remains in the liquid form. The growth terminates when the NWs are carried out of the hot zone of the furnace by means of a carrier gas flow to solidify onto a cold finger. Additionally, dopants such as diborane (B_2H_6) and red-phosphorous or phosphine can be introduced into the carrier gas to prepare p- or n-doped SiNWs, respectively.

Bottom–up VLS method for synthesis of SiNWs results in a hexagonal shaped NWs in terms of cross-section [50], which have two different exposed facets of surface crystal orientation, i.e., Si <1 1 1> and Si <0 0 1> planes [52]. The advantage of this method is that well-established phase diagrams can be used to predict catalyst and NW materials, and growth conditions for the preparation of NWs. Additionally, doping levels can be varied during the growth of SiNWs. This is important as the dynamic range of sensing using NW-FETs as a platform for biomolecular interactions depends on the material properties and doping levels [61].

2.3. Alignment of SiNWs

The bottom–up approach for synthesis of SiNWs is attractive as it results in a generation of high-quality, small diameter (3–5 nm) and single-crystalline NWs. However, in order to realize a functional FET device, the NWs require assembly with controlled transfer, orientation and density on a device substrate for subsequent integration with the circuitry in a spatially-defined manner. A number of methods have been reported in the literature that allow for controlled alignment and assembly of 1-D SiNWs into desired architectures. These methods include Langmuir–Blodgett (LB), blown–bubble (BB), microfluidic flow, electric field and contact printing alignment. The underlying theme of these methods is to provide well-defined and controlled assembly of individual NWs on device substrates that will subsequently be used for the development of functional multiplexed arrays using top–down lithography.

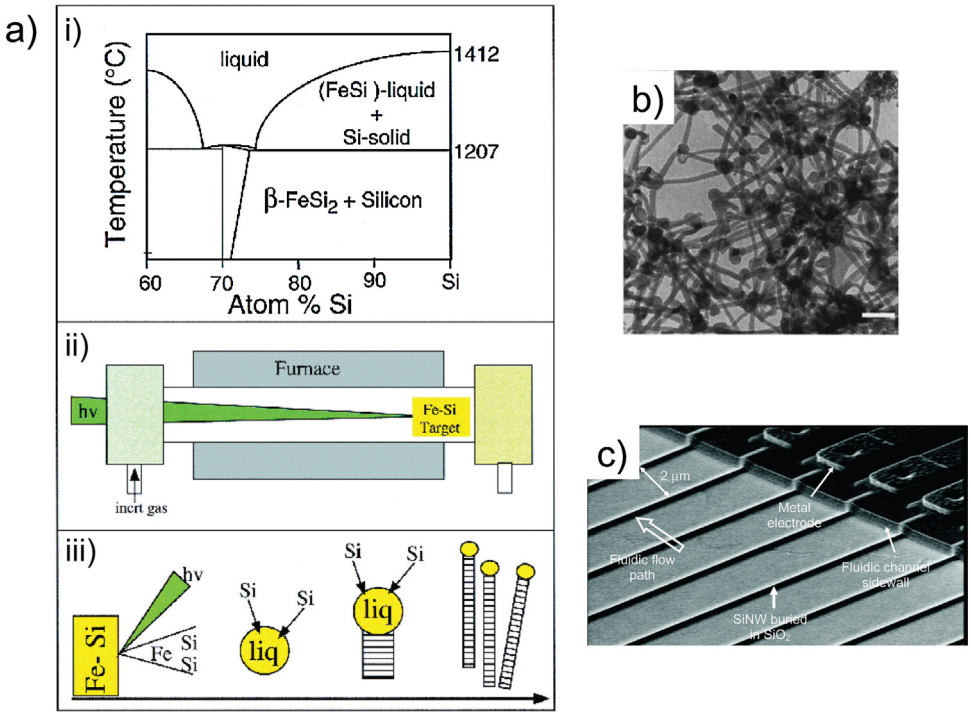

Fig. 2. (a) Synthesis of SiNWs using a bottom–up approach. (i) Phase diagram for Fe–Si binary system. (ii) Schematic of an apparatus for synthesis of SiNWs using VLS growth and laser ablation cluster formation method. (iii) Growth profile for the synthesis of SiNWs. The black arrow indicates the progress of growth. (b) TEM image of SiNWs that were synthesized via the bottom–up approach using VLS growth mechanism. The white scale bar represents 100 nm. (c) SEM image of SiNWs fabricated using the top–down approach. Panels (a) and (b) reprinted with permission from reference [28]. Panel (c) reprinted with permission from reference [48].

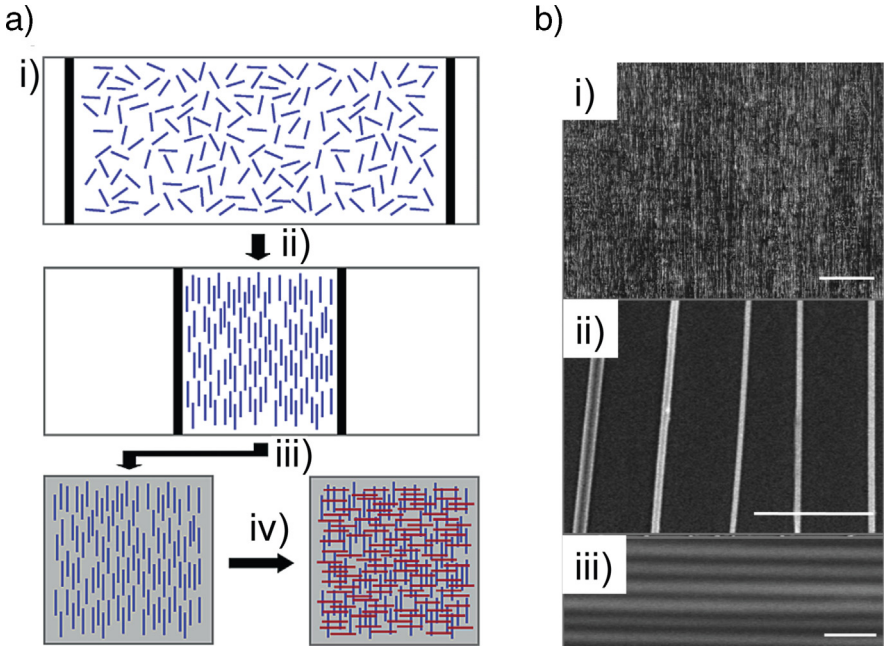

Fig. 3. (a) Schematic representation of a process flow for alignment of NWs using a LB approach. (i) The NWs (in blue) are suspended at the air–water interface and then (ii) subjected to compression using a LB trough to a defined pitch to result in parallel alignment of NWs. (iii) The NWs are then transferred to a substrate to yield an aligned parallel array. (iv) The aforementioned steps can be repeated again with another batch of NWs (in red) to yield a crossed NW structure. (b) (i) SEM image of aligned parallel SiNWs formed using a LB technique. The scale bar represents 100 μm. SEM images of aligned parallel SiNWs with inter-NW spacing at (ii) ca. 0.8 μm and (iii) 90 nm. The scale bars in (ii) and (iii) correspond to 1 μm and 200 nm, respectively. Figures reprinted with permission from reference [62] (For interpretation of the references to colour in this figure legend, the reader is referred to the web version of this article.).

2.3.1. Langmuir–Blodgett alignment

In the process of LB alignment, the NWs are suspended at the air–water interface by means of surfactants that can coordinate with the NW surface (e.g., 1-octadecylamine) as shown in Fig. 3a(i). The NWs are then subjected to uniaxial compression using a LB trough. This procedure results in the formation of a close packed monolayer of NWs, with the NWs oriented parallel to each other (Fig. 3a(ii)). The NWs are then transferred from the air/water interface to a planar substrate to produce an array of NWs (Fig. 3a (iii)) [37]. The inter-NW spacing can be varied from μm to several nm by controlling compression using the LB trough (Fig. 3b) [62]. LB alignment of NWs is suitable for patterning large areas (several cm) and it is amenable to the development of hierarchical structures (e.g., crossed NWs as shown in Fig. 3a(iv)) by patterning of independent sequential layers.

2.3.2. Blown–bubble alignment

In the process of BB alignment, a homogenous suspension of NW-polymer solution with viscosity in the range of 15–25 Pa s is blown into a bubble film using a gas flow as depicted in Fig. 4 [63]. The transfer of the aligned NW film to a substrate is done by a physical contact between the BB film of NWs and the substrate during the expansion of the bubble. The inter-NW separation distance (from 3 μm to 50 μm) and the density of aligned NWs (from 4×10^4 NW cm^{-2} to 4×10^6 NW cm^{-2}) can be tuned by modulating the concentration of NWs in the suspension [63]. The blown–bubble method is advantageous for patterning and alignment of NWs over large areas (mm to m range) and this method is also amenable to patterning of a broad range of substrates (planar, curved and flexible substrates).

2.3.3. Microfluidic flow alignment

Parallel alignment of NWs up to mm length scale using a microfluidic flow was demonstrated by Huang et al. [64]. The microfluidic chip consisted of a hybrid of a polydimethylsiloxane (PDMS) cover and a planar silicon (SiO_2/Si) substrate, where the surface of silicon was modified with amine functionality using 3-aminopropyltriethoxysilane (APTES) to facilitate adsorption of

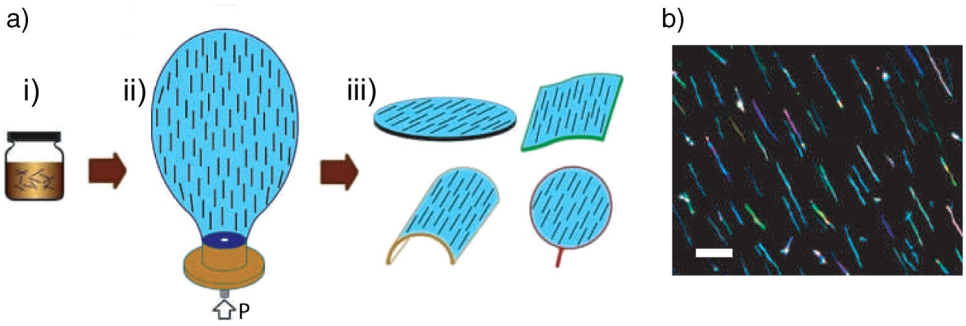

Fig. 4. (a) Schematic of the steps for the alignment of solution-phase NWs using a BB method. (i) A homogenous suspension of NW-polymer solution is (ii) blown into a bubble using a gas flow at pressure *P* using a circular die. (iii) A film of NWs is then transferred to planar or curved substrates during the expansion phase of the BB by a physical contact. (b) Dark-field optical image of aligned NWs using blown–bubble alignment. The scale bar represents 10 μm. Figure reprinted with permission from reference [63].

solution-phase NWs. The angular distribution of the aligned parallel NWs with respect to the flow direction was tunable by the flow rate (Fig. 5c). These results suggested that the shear forces that were generated as a result of microfluidic flow were responsible for the alignment of SiNWs. Moreover, the surface coverage of NWs on the planar substrate could be controlled by the duration of the flow (Fig. 5d). As an example, a flow duration of 30 min under a constant flow rate provided a density of ca. 2–3 NWs per μm, which corresponded to an average inter-NW separation distance of 400 nm. The authors also reported that the SiNWs could be patterned into different arrangements that mimicked the surface pattern of an amine-terminated surface. It should be noted that surface chemical patterning in the absence of fluidic flow provided poor control of the alignment of SiNWs, resulting in looping and bridging of SiNWs around chemically patterned areas. Moreover, higher order hierarchical structures of SiNWs such as cross-bar arrays and equilateral triangles could also be obtained using layer-by-layer assembly with different flow directions for sequential steps [64].

2.3.4. Electric-field alignment

Electric-field mediated alignment of NWs is attractive as it allows for control of the positioning of individual NWs into specific chip/device locations. Additionally, these methods require smaller amounts of NWs as compared to LB and microfluidic flow assembly of NWs [61]. Freer et al. reported the assembly of single NWs at 16,000 patterned electrode sites over an area of 400 mm^2 using dielectrophoresis within flow channels [65]. This method for the assembly and alignment of NWs combined the conventional top–down microfabrication techniques with the high-precision bottom–up alignment of NWs. A solution of NWs was hydrodynamically injected into a flow channel. The quartz surface of the channel was patterned with electrodes by standard photolithography/etching techniques and the electrodes allowed for an application of AC electric field. The NWs that were within the decay length of the AC electric field were subjected to polarization and therefore attracted to the electrodes. The balancing of the opposing dielectrophoretic and hydrodynamic drag forces resulted in the entrapment of NWs at the electrodes. For the areas of the microfluidic channel that were without patterned electrodes, the double-layer electrostatic repulsive forces between the NWs and surface charge prevented "non-specific" interaction of NWs with the surface. The electric field gradient resulted in the alignment of NWs parallel to the electric field gradient.

The assembly of single NWs at the patterned electrodes required a balance between the dielectrophoretic and hydrodynamic forces (Fig. 6a and b). For example, for a constant flow rate of 1.3 mL min^{-1}, two NWs were stable at a single electrode site at an applied voltage of ca. 404.5 mV. Reduction in the applied voltage to a value of 381.5 mV resulted in an assembly of single NWs at the electrodes. Further reduction in the applied voltage to a value below 270 mV resulted in the release of any NWs at the electrodes (Fig. 6a). Assembly of greater than two NWs at a particular electrode site required an application of voltage that was greater than 404.5 mV. The results demonstrated that an increase of the applied voltage was commensurate with the strength of dielectrophoretic forces, resulting in a greater number of NWs assembled on a particular electrode. In order to lock individual NWs at the electrode sites, excess NWs from the flow channel were first removed by flushing the flow cell with the solvent (mixture of isopropylalcohol and water), followed by increase of voltage to 7 V. Overall, the authors reported 98.5% yield of the alignment of single NWs at 16,384 electrode sites with sub-micron resolution using the combination of dielectrophoresis and hydrodynamic flow (Fig. 6c).

Electric-field mediated bottom–up assembly of NWs combined with the top–down microfabrication of circuitry was also reported by Li et al. [66]. The authors used three different mechanisms, which included electric fields, capillary forces and NW lift-off, in order to achieve a high-yield of NW assembly over a cm length scale. Arrays of wells were fabricated in an insulating photoresist layer that covered the metal guiding electrodes on the chip surface (Fig. 6d(ii)). An alternating voltage in the kilohertz range was applied between the guiding metal electrodes in order to polarize the NWs in suspension. The dielectrophoretic force that resulted from the AC electric field spatially confined the NWs, resulting in

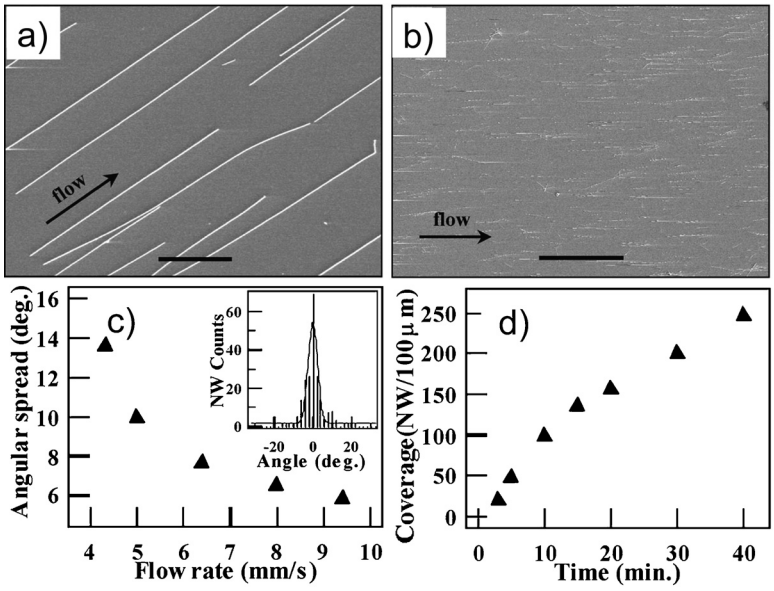

Fig. 5. Parallel alignment of NWs using a microfluidic flow. (a and b) SEM images of parallel arrays of NWs aligned by a microfluidic flow. Scale bars in (a) and (b) correspond to 2 μm and 50 μm, respectively. (c) NW angular spread with respect to the flow direction as a function of the flow rate. Each data point in the figure corresponds to a statistical analysis done on ca. 200 NW. Inset shows histogram of angular distribution of NWs at a flow rate of 9.40 mm/s. (d) Effect of flow duration on the average density of NWs at a flow rate of 6.40 mm/s. Figure reprinted with permission from reference [64].

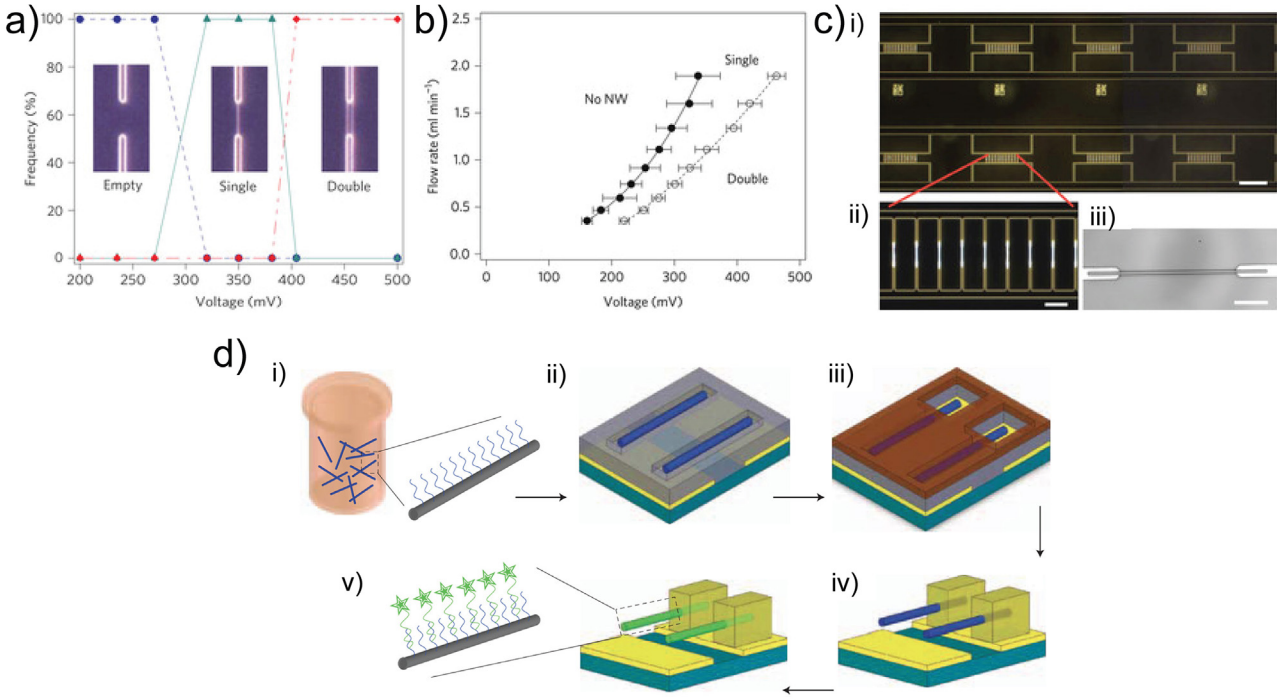

Fig. 6. Assembly of NWs at the patterned electrode sites using dielectrophoresis. (a) Effect of the voltage on the frequency of the occurrence of empty electrodes (circles), a single NW (triangles) and double NWs (diamonds) at the patterned electrode sites under a constant flow rate. AC frequency and flow rate were 500 Hz and 1.3 mL min^{-1}, respectively. (b) Effect of voltage and flow rate on the assembly of no NW, single NW and double NWs at the electrode sites. (c) Optical dark-field images of the assembly of single NWs at (i) 8 patterned electrode arrays and (ii) single electrode array. (iii) Deep-UV image of a single NW at a single electrode site. (d) Process-flow diagram for assembly of single NW resonator arrays. (i) NW surface modified with PNA probe. (ii) Assembly of single NWs inside wells patterned in photoresist layer using dielectrophoresis. (iii) Deposition of second photoresist layer with a clamp window. (iv) Electrodeposition of metal clamps at the NW tip and removal of photoresist layers to suspend the clamped NWs. (v) Hybridization with fluorescently labeled oligonucleotide targets with the PNA probes immobilized on the NW surface. The methodology can be extended to the assembly of NW-FET devices. Panels (a)–(c) reprinted with permission from reference [65]. Panel (d) reprinted with permission from reference [66].

an alignment of NWs along the electric field gradient. Further confinement of the NWs that were preferentially retained in the wells was achieved via capillary forces that resulted upon evaporation of the solvent within each well. The dimensions of each well determined the height of the NWs that could be suspended in photoresist wells. A second photoresist masking layer was then deposited on top of the confined NWs with a window at one end (Fig. 6d(iii)). The window area that exposed one end of the confined NW was subsequently used for electrodeposition of the metal clamp (Fig. 6d(iv)). The photoresist layers were then dissolved, which allowed for removal of any misaligned NWs, resulting in parallel arrays of free-standing NW cantilevers (Fig. 6d (v)). The authors reported 80% yield in terms of alignment of single NWs assembled in arrays of over 2000 resonators.

An important aspect of this work was that the chemical functionalization of NWs was done off-chip, which allowed for the use of optimized conditions for surface functionalization of NWs. Additionally, assembly of single NWs and subsequent fabrication steps were done in the absence of chemical etchant, which could potentially otherwise degrade the integrity of the receptor chemistry for selective interaction. As a proof-of-concept, the authors modified the surface of NWs with peptide nucleic acid (PNA) probes for selective detection of oligonucleotide targets that served as markers for hepatitis C and hepatitis V viruses. The modification was completed prior to the integration of probe-modified NWs on the chip. Hybridization with fully-complementary (FC) and non-complementary oligonucleotide (NC) targets showed that the immobilized probes retained their functionality. The authors reported that the methods presented in their work are applicable to the assembly of single NWs for the development of NW-FET devices.

2.3.5. Contact printing alignment

In addition to the aforementioned methods for the alignment and assembly of solution-phase NWs, methods for the assembly of dry NWs on device substrates have also been reported. These methods are based on printing methods, where a monolayer of NWs (synthesized via nanocluster mediated VLS growth) is transferred directly from a growth substrate (donor substrate containing “lawn” of NWs) to a receiver substrate using either contact printing (Fig. 7a) or roll-transfer printing (Fig. 7b). In the case of contact printing, the transfer of NWs from a donor substrate to a lithographically patterned (e.g., photoresist layer) receiver substrate is mediated by shear forces that are generated during the directional sliding (20 mm min^{-1}) of the two substrates against each other under a gentle pressure [58,67]. The improvement in alignment yield and mitigation of uncontrolled breakage of NWs during the sliding process can be afforded by an application of lubricant between the two sliding surfaces [67]. In case of roll-transfer printing, the donor substrate containing vertically aligned NWs and a stamp (e.g., PDMS) are subjected to printing using a roller. During this process, the NWs are transferred from a donor substrate to a stamp, where the horizontal alignment of the NWs is governed by the rolling direction. The roll printing step is repeated again between the stamp and a receiver substrate to transfer the aligned NWs from the stamp to a receiver substrate [68]. The transfer efficiency and alignment yield of NWs using printing methods depend on factors such as strength of bonding between the donor substrate and NW and the physical characteristics (e.g., elasticity) of the stamp [68]. The elastomeric nature of PDMS (strained PDMS and subsequent release) has also been used to improve the alignment yield (from 25 to 88%) and density of NWs (by 75%) during the stamp transfer step via contact printing

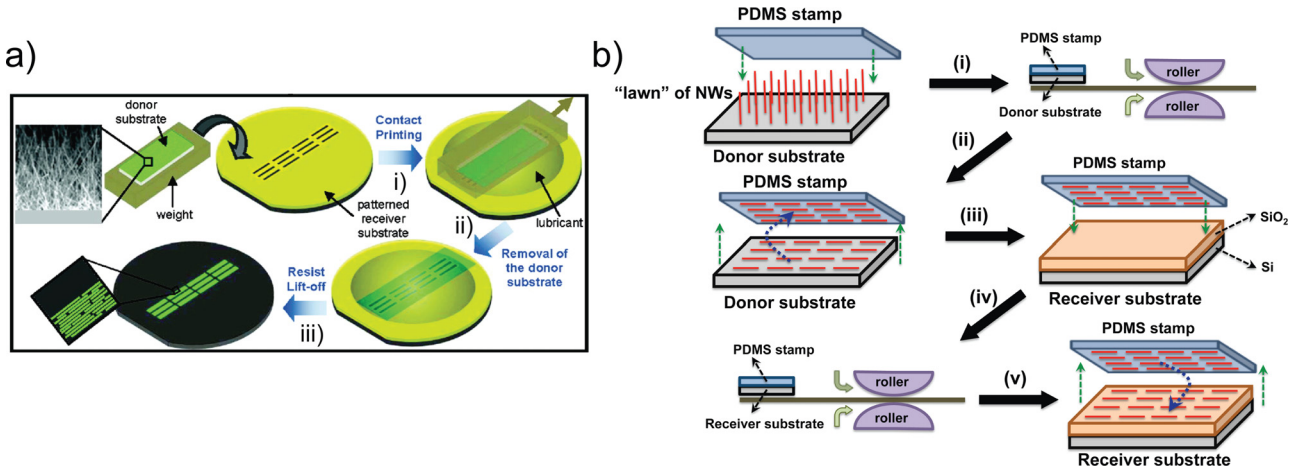

Fig. 7. Schematic representation of the steps for alignment of NWs using (a) contact printing and (b) roll-transfer printing. (a) (i) A photoresist patterned receiver substrate is subjected to directional sliding (green arrow) with the donor substrate containing a "lawn" of NWs under gentle pressure (ca. 10–20 g cm^{-2}, shown as weight). (ii) The donor substrate is then removed from the receiver substrate. (iii) The photoresist layer is dissolved away leaving horizontally aligned NWs on the receiver substrate. (b) The donor substrate and stamp are subjected to (i) roll printing resulting in transfer of NWs to the stamp. (ii) The stamp is then removed from the donor substrate. (iii) The NW-printed stamp is placed against a receiver substrate and subjected to another round of (iv) roll printing. (v) Removal of stamp from the receiver substrate with horizontally aligned NWs on the receiver substrate. Panel (a) reprinted with permission from reference [67] and panel (b) adapted from reference [68] (For interpretation of the references to colour in this figure legend, the reader is referred to the web version of this article.).

[69,70]. Table 2 provides a comparison of various methods for the alignment of NWs.

2.4. Surface functionalization

Functionalization of surfaces with receptor molecules (bio-recognition element) is an important step for the development of bioprobes and biosensors. SiNWs when exposed to atmospheric conditions develop a native oxide layer (1–2 nm thick) of SiO_2. Methods for surface modification of oxide surfaces, such as planar glass and silicon oxide, are well established [25,37]. Methods for surface modification of SiNWs commonly make use of silane coupling agents (organosilanes) in order to introduce various functional groups such as thiols [71–73], epoxides [74], aldehydes [7,17,48,75] and primary amines [3,76–78] on the SiNW surfaces. As shown in Fig. 8a, such modification simplifies subsequent conjugation of biomolecules such as oligonucleotides and proteins.

The most commonly implemented silane coupling agents that have been reported in the literature for immobilization of PNA/DNA probes and capture antibodies on the surface of SiNWs are APTES, 3-mercaptopropyltrimethoxysilane (MPTMS) and 3-(trimethoxysilyl) propyl aldehyde for introduction of primary amine, thiol and aldehydes functionalities to the surface of SiNWs, respectively [3,72,76]. As shown in Fig. 8b(i), surface modification of SiNWs with APTES results in an amine-terminated surface (Step 1), which can subsequently be modified with dialdehyde (glutaraldehyde) via imine formation to yield an aldehyde termi-nated surface (Step 2). It should be noted that glutaraldehyde is a homo-bifunctional linker and has the potential to bridge two amine functional groups. This possibility can be ameliorated by using a high concentration of glutaraldehyde (5–10% (v/v)) [80]. Imines (Schiff base formation) can be reduced *in situ* to form secondary amines by treatment with sodium cyanoborohydride ($NaCNBH_3$) [22]. This step is important as immobilization by Schiff base formation has been linked to the time-dependent loss of surface functionality owing to the labile nature of the Schiff base [79]. Aldehyde terminated SiNWs can subsequently be modified with amine-terminated DNA/PNA or proteins (via lysine residues) to achieve immobilization of biomolecules.

The oxide layer that develops on the surface of SiNW is useful for surface functionalization using various methods of silane chemistry. However, this oxide layer concurrently serves as a dielectric layer, screening the core of the SiNW from the surface charge that develops on the SiNW upon biomolecular interaction, thereby reducing the sensitivity of the device [76,81]. The thickness of the oxide layer is commensurate with the decrease in device sensitivity [54,79]. This oxide layer can also result in the degradation of analytical performance due to the presence of interfacial electronic trap states [76,82]. Moreover, when the oxide layer is used for surface functionalization, it reduces the extent of selective binding of analyte on the NW surface by means of a dilution effect. The oxide layer most often coats the entire device substrate area, leading to immobilization of selective chemistry everywhere on the device substrate rather than only on NWs [21,81,83]. This effect has been reported to reduce the sensitivity and response time of the assay owing to the binding competition of sites that are not associated with the NWs [84]. The sensitivity of a device can be improved using surface modification methods that allow for replacement of the native oxide layer with a molecular layer that is thinner than the oxide, and that results in selective surface functionalization of NWs with the desired recognition element.

It has been reported that hydrogen-terminated (H-terminated) SiNWs that are passivated with alkyl groups exhibit low interfacial trap states, improved resilience to oxidation, higher conductance response and hence offer improved FET performance [52,85,86]. As a result, another surface chemistry for introducing amine functionality and subsequently aldehyde functionality to the surface of H-terminated SiNWs is based on a UV-initiated hydrosilylation reaction as shown in Fig. 8b(ii). Monolayers based on hydrosilylation reaction have been reported to be more reproducible and stable than silane-based monolayers [54,87]. The first step in this reaction scheme involves a removal of the oxide layer from the surface of a SiNW to yield H-terminated SiNW. This is done using sequential treatment with hydrofluoric acid and ammonium fluoride (Step 1). The next step involves UV-initiated hydrosilylation reaction of H-terminated SiNW with tert-butyl allylcarbamate (Boc-protected primary amine with an alkene group at the end of alkane chain) (Step 2). In order to yield a primary amine, deprotection of the Boc-protected primary amine is done using sequential treatment with trifluoroacetic acid and ammonium hydroxide (Step 3). Step 4 in Fig. 8b(ii) is the same as

Table 2
Comparison of various methods for alignment of NWs.

	Alignment method	Inter-NW distance, alignment yield and control of NW density	Advantages	Disadvantages	References
Langmuir–Blodgett alignment	Parallel alignment of NWs during uniaxial compression of LB trough.	8–10 NW/μm; Alignment yield: ca. 80–90%. NW density is controlled by the compression of LB trough and/or by etching of silicon oxide layer.	Alignment can be applied to substrates spanning several cm^2 in area. Alignment method applicable to many NW materials. Cross-NW structure is possible using sequential rounds of LB alignment.	Irreproducibility in the alignment direction of NWs, resulting in poor end-to-end registration with the source and drain electrodes. Requirement of large sample volume of NWs (mL). Only suitable with NWs with diameter > 15 nm [58,61]. Difficult to control the number of NWs bridging the source and drain contact electrodes.	[62]
Blown–bubble alignment	Suspension of NW-polymer solution blown into a bubble using gas flow.	ca. 1 NW/3 μm; Alignment yield: ca. 90%. NW density is controlled by changing the concentration of NWs in the NW-polymer suspension solution.	Alignment method can be applied to various NW materials and to various substrates (planar, plastic, curved etc.). Alignment feasible up to various length scales (from mm to m).	Requires surface functionalization of NWs with epoxy group to form NW-polymer film, which may limit the availability of NW surface for immobilization of biorecognition element. Requirement of large sample volume of NWs (mL). Difficult to control the number of NWs bridging the source and drain contact electrodes.	[63]
Flow-based alignment	Microfluidic flow driven shear forces, where the adsorption of NWs is facilitated by surface charge.	2–3 NWs/μm; Alignment yield: ca. 80%. NW density is controlled by flow duration.	Complex NW structures, such as cross-NW arrays and equilateral triangles, are possible using a chemically patterned surface and sequential layer-by-layer assembly steps with different flow directions. Alignment requires small sample volume of NWs (μL).	Alignment limited to planar substrates and to small length scales (mm to cm). Only suitable with NWs with diameter > 15 nm [58,61]. Difficult to control the number of NWs bridging the source and drain contact electrodes.	[64]
Electric-field based alignment	Balance of hydrodynamic and dielectrophoretic forces.	1 NW/12 μm; Alignment yield: >98%. NW density is governed by the number of patterned electrode sites in a given area.	No integration issues of NWs with the source and drain contact electrodes (high yield of alignment >98%). Surface modification of NWs can be done prior to alignment. Alignment requires small sample volume of NWs (μL). Each NW can be addressed individually from an electrical contact standpoint.	Requires precise control of the hydrodynamic and dielectrophoretic forces. Variations in the physiochemical properties of NWs can impede the alignment. Alignment limited to small area (from mm^2 to cm^2). Yields lower NW density as compared to other methods.	[65,66]
Contact printing alignment	Shear stress during the sliding of donor (the growth substrate) and receiver substrates. An intermediate step such as stamp transfer using a roller can also be employed (roll-transfer printing) [68].	4–8 NW/μm; Alignment yield: 80–90%. NW density can be controlled by modifying the receiver substrate with different functional groups and/or by controlling the NW density on the growth (donor) substrate.	Alignment feasible with various NW materials and is applicable to diverse substrates (silicon, plastic and rubber etc.). Applicable to NWs with diameter <15 nm. Multilayer functional device structures are possible by iterative contact printing and device fabrication steps. Roll-transfer printing method can be operated in a continuous fashion. Strained PDMS stamp can be used to improve alignment yield and NW density.	Uncontrolled breakage of NWs during the transfer process, resulting in distribution of NW lengths (can be mitigated by an application of lubricant). The length of NWs printed on the receiver substrate is typically less than the length of NWs on the growth substrate. Difficult to control the number of NWs bridging the source and drain contact electrodes.	[58,67–70]

Step 2 in Fig. 8b(i) and yields an aldehyde terminated SiNW surface. This method for surface modification of SiNWs is advantageous as it not only offers selective surface functionalization of only SiNWs, but also improves the electrical performance of the FET sensors [52]. Additionally, replacement of the oxide layer with an organic film is useful to reduce the extent of oxidation of Si surfaces when further exposed to air and electric fields [86,88–90].

Park et al. reported another method for selective surface functionalization of SiNWs that is based on localized nanoscale Joule heating of prefabricated NWs that were covered with a protective polymer layer of polytetrafluoroethylene [91]. An application of electrical bias to a chosen NW resulted in an ablation of the protective polymer layer owing to the resulting Joule heating. A subsequent low power O_2 plasma treatment then allowed for the modification of the NW surface with an organosilane film to immobilize biomolecules. Bunimovich et al. reported an electrochemical method for selective functionalization of H-terminated silicon surfaces that were modified with an electroactive monolayer of hydroquinone [54]. Functionalization of selected NWs was achieved following oxidation of hydroquinone to benzoquinone by an application of electrical potential (ca. 700 mV versus Ag/AgCl) via Michael addition of molecules that presented a thiol group. In addition, selective surface modification of SiNWs for immobilization of a biorecognition element has also been achieved prior to the assembly of NWs on a device substrate. Examples include surface modification of SiNWs with an APTMS

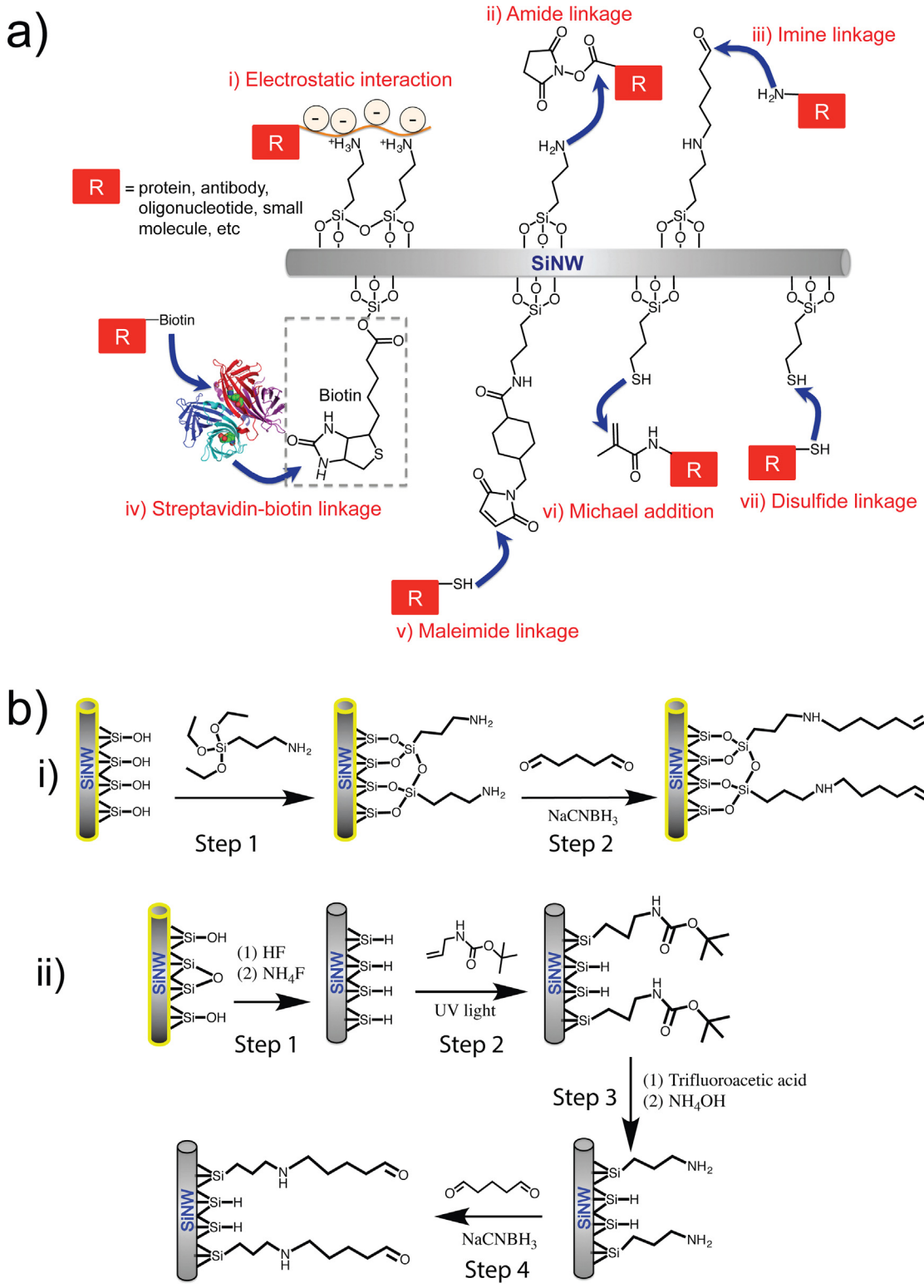

Fig. 8. (a) Selected conjugation strategies that have been reported with SiNWs. (i) Electrostatic association [76], (ii) amide coupling via activated ester formation [53], (iii) imine formation (Schiff base) that can be reduced *in situ* to a secondary amine using $NaCNBH_3$ treatment [75,79], (iv) streptavidin-biotin based affinity interaction [8,52], (v) maleimide activation and linkage [78], (vi) Michael addition [72] and (vii) disulfide linkage [71]. Figure not to scale. (b) (i) Surface modification of SiNWs with aldehyde functionality by utilizing the exposed oxide layer (shown in yellow color along the periphery of a SiNW). Surface silanol groups on SiNWs are modified with APTES to yield a primary amine terminated surface (Step 1). Subsequent treatment with glutaraldehyde provides an aldehyde terminated surface *via* imine formation, which can be reduced *in situ* to a secondary amine using $NaCNBH_3$ treatment (Step 2). Aldehyde groups can subsequently be used for immobilization of either amine terminated DNA/PNA or proteins via lysine residues. (ii) Removal of an oxide layer and UV-initiated hydrosilylation reaction scheme for introducing primary amine functionality on the surface of SiNWs. Step 1: Removal of oxide layer (shown in yellow color along the periphery of a SiNW) from the surface of SiNW to form H-terminated SiNW surface. Step 2: UV-initiated hydrosilylation reaction using a Boc-protected allylamine. Step 3: Deprotection of primary amine. Step 4: Introduction of aldehyde functionality using imine formation and *in situ* reduction to secondary amine. Aldehyde groups can subsequently be used for immobilization of either amine terminated DNA/PNA or proteins via lysine residues (For interpretation of the references to colour in this figure legend, the reader is referred to the web version of this article.).

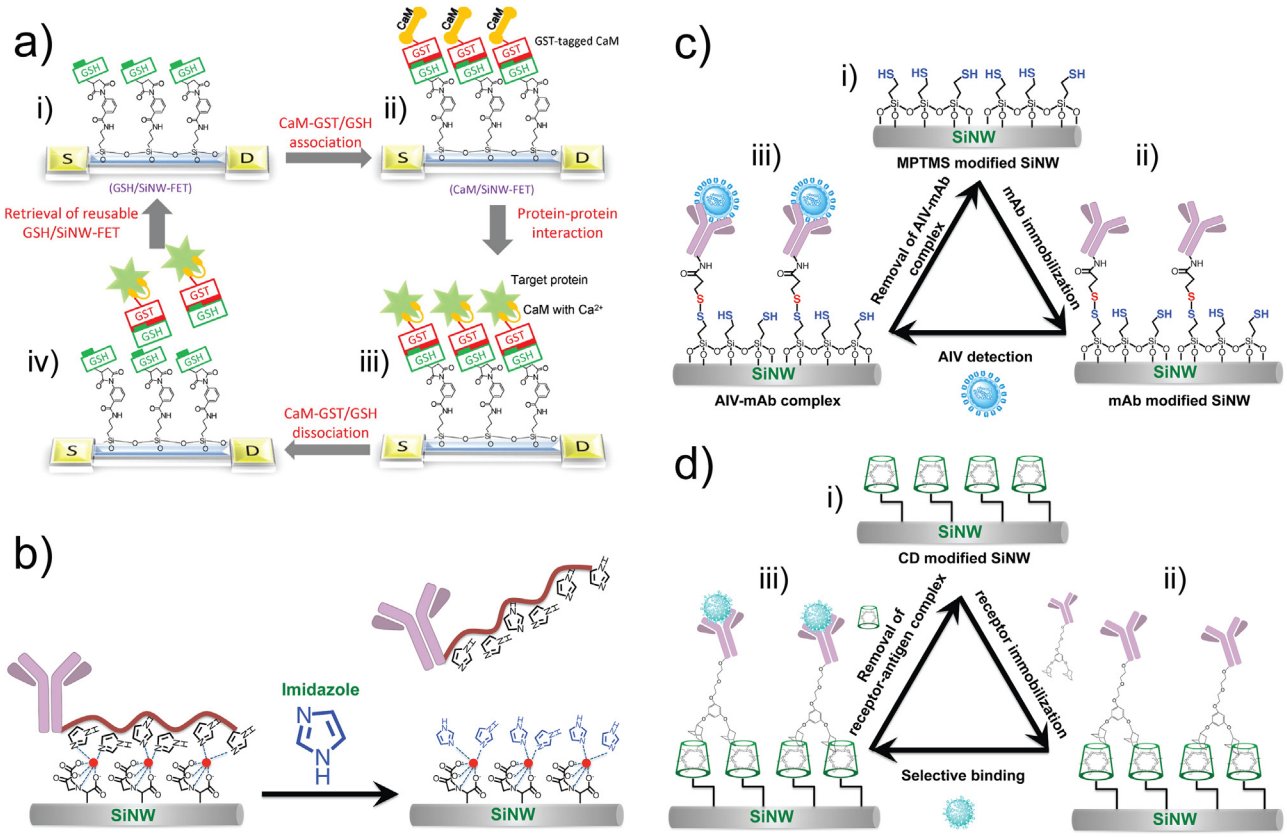

Fig. 9. Interfacial chemistries for reusable SiNW-FET sensors based on (a) GSH/GST interaction, (b) His-tag/Ni^{2+}:NTA interaction, (c) cleavable disulfide bond formation and (d) β-CD–Ad interaction. (a) (i) GSH modified SiNW surface is subjected to the (ii) immobilization of GST tagged CaM via GSH/GST interaction. (iii) Ca^{2+} dependent CaM and target protein interaction. (iv) Dissociation of GSH/GST interaction by an application of GSH solution (≥1 mM) to yield GSH terminated surface as in (i). (b) Immobilization of His-tag appended antibody using SiNW surface that is functionalized with Ni^{2+}:NTA motif. The His-tag/Ni^{2+}:NTA interaction is disrupted by washing the surface with a solution of imidazole (≥500 mM). Histidine residue (black); imidazole (blue); Ni^{2+} ion (red sphere). (c) (i) MPTMS modified SiNW surface (thiol terminated) is subjected to the (ii) immobilization of monoclonal antibody (mAb) by disulfide bond formation. After AIV-mAb complex formation in (iii) the surface of a SiNW is reverted to (i) by cleavage of a disulfide bond by an application of DDT solution (500 mM). (d) (i) β-CD modified SiNWs is subjected to the (ii) immobilization of selective agent via β-CD–Ad interaction. Following selective interaction in (iii) the surfaces of SiNWs are reverted to (i) by an application of a 8 mM solution of β-CD. Panel (a) reprinted with permission from [98], panel (b) adapted from [74], panel (c) adapted from [71]. Figures not to scale (For interpretation of the references to colour in this figure legend, the reader is referred to the web version of this article.).

film [84] and immobilization of PNA probes on the surface of SiNWs [66]. It should be noted that selective functionalization of NWs is important to not only improve the sensitivity of the assay, but also for the development of multiplexed assays which require functionalization of different NWs with different selective agents.

2.4.1. Reusable interfacial chemistries

Interfacial chemistries for the development of reusable SiNW-FET sensors have been reported. Reuse of NW-FET sensors ameliorates issues of batch-to-batch variation associated with the fabrication of NW sensors and expedites calibration of the device prior to measurements. Two general routes for the development of reusable interfacial chemistries for NW-FET sensors are: (1) well-known protein purification systems that use reversible association–dissociation interaction of affinity-based recognition motifs [92,93] and (2) chemical linkers that are cleavable [21,71]. Immobilization of biomolecules via affinity-based recognition motifs allows for control of the structural orientation of the interfacial chemistry [94], a reduced probability of denaturation of selective agent upon surface immobilization, and improved availability of selective chemistry to interact with the target analyte [95,96]. An affinity-based reversible interaction that relies on binding between glutathione (GSH) and glutathione S-transferase (GST) was reported by Lin et al. (Fig. 9a) [97]. The surface of a SiNW was modified with GSH to which GST was subsequently conjugated via affinity interaction. Immobilization of selective agent (biotin) was mediated by a construct that consisted of biotin-derivatized antibody against GST for selective detection of streptavidin. Alternatively, a fusion protein construct consisting of GST tagged to another protein recognition motif (such as calmodulin (CaM), a Ca^{2+} chelating protein) can also be used for conjugation to a GSH modified NW surface (Fig. 9a(ii)) [98,99]. In order to regenerate the surface, i.e., removal of GST linked to biotin-derivatized antibody against GST, the surface was washed with 10 mM GSH. Although the GSH/GST reversible binding system has been used to study protein–protein interactions [98,99], a significant limitation of this system is the large separation distance between the NW surface and the target–receptor complex (size of GST ca. 2.5 nm [100]) with a concomitant decrease in the sensitivity of the assay (LOD in nM range and 1–2 orders of magnitude dynamic range) [97,98].

Liu et al. reported another affinity-based reversible surface functionalization of SiNWs with proteins using histidine tag/Ni^{2+}:nitrilotriacetic acid (His-tag/Ni^{2+}:NTA) interaction as shown in Fig. 9b [74]. The surface of a SiNW was functionalized with Ni^{2+}:NTA motif for immobilization of proteins that were appended to His-tag. The His-tag/Ni^{2+}:NTA interaction could be disrupted either by washing the surface with imidazole or by introduction of ethylenediaminotetraacetic acid (EDTA). Imidazole competes with the His-tag in terms of coordinating with Ni^{2+}, while the presence

of EDTA results in a sequestration of Ni^{2+} ions, which leads to disruption of His-tag/Ni^{2+}:NTA interaction. As compared to the GSH/GST reversible binding system, the His-tag/Ni^{2+}:NTA system offers a short separation distance between the NW surface and the selective interface. This can improve the sensitivity of NW-FET sensors by reducing the extent of charge screening.

Chiang et al. reported the use of disulfide linker for reversible surface functionalization of SiNWs as shown in Fig. 9c [71]. The surface of a SiNW was functionalized with MPTMS to which monoclonal antibody (mAb) against avian influenza virus (AIV) was coupled via disulfide bond formation. After the detection of AIV particles via the formation of the AIV-mAb complex, the NW surface was reverted to a thiol terminated surface by washing the surface with dithiothreitol (DTT). Alternatively, *tris*(2-carboxyethyl) phosphine (TCEP) can also be used to reduce the disulfide bond [21].

Duan et al. reported another interfacial chemistry for the development of reusable SiNW-FET sensors based on reversible interaction between β-cyclodextrin (β-CD) and adamantane (Ad) groups [101]. As shown in Fig. 9d, the surface of SiNWs was functionalized with a monolayer of β-CD to which divalent Ad groups were attached via adsorption. The interaction between β-CDs and Ad groups was destabilized by using a competitive desorption approach by washing the surfaces of SiNWs with a 8 mM solution of β-CD. This treatment resulted in complete desorption of Ad groups from the surface of β-CD modified SiNWs. The reversible interaction between β-CDs and Ad groups was used for selective detection of streptavidin by modifying the surfaces of SiNWs with a linker that consisted of two Ad groups attached to a biotin functionality. Ad groups were used to immobilize biotin on the surface of a SiNW via β-CD–Ad interaction. Additionally, three oligo(ethylene glycol) chains were incorporated in the linker to promote water solubility of the linker and to minimize non-specific adsorption of streptavidin.

2.5. Charge screening and Debye length

Ionic strength is an important consideration that affects the sensitivity of SiNW-FET devices. SiNWs are field effect sensors that respond to changes in surface charge or electric field that are introduced by analyte binding. In aqueous solution, the surface charge attracts counterions forming an electric double layer that screens the surface charge. The physical distance of such charge screening is characterized by the Debye length [22,23]. With increasing ionic strength of the solution, the electrical double layer and the Debye length compress due to charge screening by counter ions, which reduces the sensitivity of the device. It is the charge-density changes that take place within the Debye length (λ_D) from the surface of the sensor that are able to significantly influence the gate voltage [22]. The Debye length corresponds to a distance from a charged surface at which the surface potential drops to $1/e$ of its initial value owing to the charge screening by the counterions, with the screening being modeled as an exponential decay function. Debye length is dependent on the ionic strength of a solution and Debye length decreases as the ionic strength of the solution increases, as can be seen by Eq. (1):

$$\lambda_D = \left(\varepsilon k_B \times \frac{T}{q^2 c}\right)^{1/2} \quad (1)$$

where λ_D is the Debye length, ε is dielectric permittivity of the media, k_B is the Boltzmann constant, T is absolute temperature, q is the charge on an electron, and c is ionic strength of the solution.

Due to a dependence of the Debye length on the ionic strength of the solution, FETs exhibit poor sensitivity in biological samples such as serum [25]. Consider an oligonucleotide hybridization reaction that takes place on the surface of a FET device that is modified with 10 base length of capture probe that binds to a 10 base target to form a 10 base pair (BP) hybrid. A diagram showing that hybrids can be oriented orthogonal to the surface of a field-effect sensor is represented in Fig. 10. The diagram shows that with increasing ionic strength of a solution the length of the DNA hybrid that remains within the Debye length decreases. For physiological solutions with ionic strength in the range of 100–150 mM ($\lambda_D < 1$ nm), it can be seen that the majority of the electric field associated with the DNA will be screened by counterions and will not influence the surface potential of a NW. If immobilization of capture probes is done via a linker, the issue of charge screening and its effect on device sensitivity becomes even pronounced. It should be noted that the aforementioned discussion assumes that the probe–target duplex is oriented normal to the surface of FET sensor, and this is not necessarily the case. Due to the effect ionic strength on device sensitivity, most studies with FETs are done under conditions of low ionic strength (10 mM) [25]. Various strategies have been reported in the literature in order to overcome this charge screening limitation of FETs so as to allow for applications in physiologically relevant ionic strength conditions. A number of such strategies are described in the applications section of this review.

2.6. Effects of NW diameter, number and doping density on assay performance

Li et al. evaluated the effects of the numbers of SiNWs, and the diameter and doping density on the sensitivity of NW-FETs for immunodetection [102]. The authors employed a piezoelectric nano-manipulator inside a SEM to control the diameter and number of NWs bridging the source and drain electrodes. The surface of each NW was functionalized with antibody for human IgG (anti-hIgG) for selective detection of human-IgG (hIgG). Sample delivery was done using a microfluidic channel and

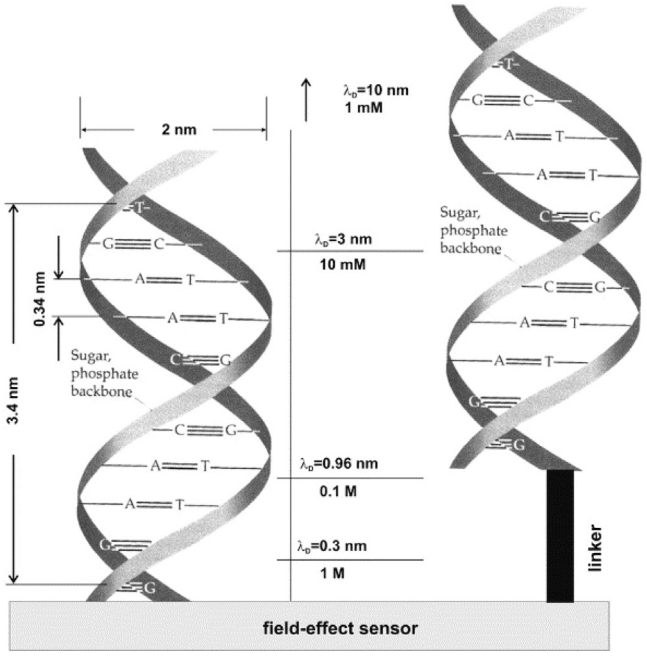

Fig. 10. Change in the Debye screening length as a function of ionic strength of a solution for a 10 BP long DNA duplex that is oriented orthogonal to the surface of field-effect sensor without (left) and with (right) a linker length of 1 nm. It can be seen that with increasing ionic strength, the fraction of DNA charge that remains within the Debye screening length decreases. Figure reprinted with permission from reference [23].

provided for a concentration range of 10 fg/mL to 10 μg/mL hIgG in 0.1 × phosphate buffered saline (PBS).

Three different permutations of the device were constructed, containing 1, 4 or 7 SiNWs bridging the source and drain. All these constructs were exposed to increasing concentrations of hIgG. The diameter and doping density of NWs were held constant at 81–100 nm and 10^{19} atoms cm^{-3}, respectively. The authors reported that the device sensitivity decreased as the number of NWs bridging the source and drain was increased. When using multiple SiNWs, the number of analyte-SiNW interactions for each SiNW is lower than would be the case if only a single SiNW were exposed to the same amount of analyte. It should be noted that this observation was only applicable for low concentrations of analyte where the analyte depletion from the sample solution upon analyte-NW interaction was significant.

Two different doping concentrations, 10^{17} and 10^{19} atoms cm^{-3}, were evaluated while keeping the SiNW diameter and number constant at 81–100 nm and 1, respectively. It was reported that the sensitivity of the device decreased as the doping density was increased. The reduction in doping concentration from 10^{19} to 10^{17} atoms cm^{-3} provided ca. 3.2 fold improvement in assay sensitivity, and 3 orders of magnitude lower LOD (10 fg/mL and 10 pg/mL for 10^{17} and 10^{19} atoms cm^{-3} doping concentrations, respectively). The highest sensitivity in terms of the conductance response of SiNW-FET is expected when the entire volume of a SiNW is field gated by charged molecules at the surface of a SiNW [53], i.e., when the screening length of the charge carriers inside a SiNW is 2–3 times greater than the radius of a SiNW [33]. An important parameter that governs the volume of SiNW that is field gated by surface charges is the density of charge carriers in silicon [33]. The NW Debye length increases with decreasing doping concentration [77], which minimized the charge screening and improved the device sensitivity.

The density of charge carriers in the SiNW can also be tuned by application of an externally applied gate voltage [33]. The "sub-threshold" regime of a transfer curve corresponds to a gate voltage at which the relative change in the conductance response of a SiNW-FET is the highest upon analyte interaction at the surface of a SiNW [33]. At this regime, the entire volume of a SiNW-FET becomes field gated by charged molecules at the surface of SiNW. This provides for effective modulation of conductance inside the SiNW by reducing the screening of charge carrier inside the SiNW. For example, Gao et al. reported a 500-fold improvement in LOD for prostate specific antigen (PSA) determination (from 0.75 pM to 1.5 fM) when the SiNW-FET sensor was operated in the sub-threshold regime as compared to a linear regime in terms of the gate voltage [33]. In the sub-threshold regime, the conductance response of a SiNW-FET varies exponentially with the gate voltage as the carrier screening length is significantly greater than the SiNW radius [33]. In the case of the linear regime, the conductance response of a SiNW-FET varies linearly with the gate voltage as the carrier screening length is smaller than the radius of a SiNW, which results in the screening of charge carriers inside the SiNW.

The performance of single SiNWs with diameters in the range of 60–80, 81–100, 101–120 nm were evaluated while keeping the SiNW doping density constant at 10^{17} atoms cm^{-3}. A negative correlation was found between device sensitivity and SiNW diameter. Analyte interaction on the SiNW surface leads to a depletion or accumulation of charge carrier over a greater cross-section of the SiNW for SiNWs of smaller diameter. Similar improvements in the sensitivity of SiNW-FET sensors have been noted for SiNWs of decreasing diameter [9,57,73]. Overall, the results of this study demonstrate that the physical properties of NWs strongly govern the sensitivity and consistency of performance of SiNW-FET devices.

3. Applications

3.1. SiNWs as ion selective nanosensors

Cui et al. reported the first example of SiNWs as chemical transducers in 2001 [3]. The authors modified p-type (boron-doped) SiNWs with an APTES film to produce pH nanosensors. The APTES was subjected to protonation or deprotonation depending on the pH of the solution, which modulated the surface charge on the SiNWs and gated the conductance of the NWs in a pH dependent manner as shown in Fig. 11a(ii). It can be seen that the NW conductance increased stepwise in a linear fashion with the increase in pH from 2 to 9, and that the conductance of the NW was constant for a given pH value. Surface modification of SiNW with APTES resulted in an introduction of primary amine functional groups in addition to the underlying surface silanol groups. At low pH, the $—NH_2$ group was protonated to $—NH_3^+$ (Fig. 11a(i)). The positive surface charge depleted the density of charge (hole) carriers in the p-type SiNW, resulting in a decrease in conductance. At high pH, the surface silanol groups were deprotonated to SiO^- (Fig. 11a(iii)), resulting in an accumulation of charge carriers in the p-type SiNW and a corresponding increase in conductance. Conductance measurements done on unmodified (without APTES) SiNWs showed a non-linear dependence on changes of pH (Fig. 11a(iv)).

Chen et al. reported that the pH sensitivity of the SiNW-FET sensor is a function of the type of functional group (pH sensitivity of methyl group < primary amine group) present on the surface of a SiNW [34]. The authors reported a near Nernstian pH response (57.8 ± 1.2 mV pH^{-1}) from SiNWs that were modified with a layer of aluminum oxide (Al_2O_3) as a gate dielectric interface, while the response from SiNWs with SiO_2-based gate dielectric interface exhibited sub-Nernstian pH sensitivity. Similarly, Dorvel at al. reported top–down fabricated SiNW-FETs with hafnium oxide (HfO_2)-based gate dielectric interfaces for pH sensing that provided response of ca. 56 mV pH^{-1} [41]. SiO_2 as a traditional top gate dielectric material has a number of shortcomings that render its FET performance inferior as compared to other high-*k* dielectric materials such as Al_2O_3, HfO_2 and tantalum oxide (Ta_2O_5). SiO_2 exhibits a relatively low dielectric constant, low pH buffer capacity and susceptibility to leakage current due to ion incorporation (e.g., proton diffusion and surface hydration) in the presence of fluids. This results in the pH sensitivity response of SiO_2 to be sub-Nernstian [41]. Replacing the SiO_2 layer with a high-*k* dielectric material allows reduction in leakage current owing to high gate oxide capacitance, which is attributed to a greater physical thickness of the gate dielectric interface without compromising the sensitivity to the surface charge [31,40,103]. It should be noted that pH sensitivity of NW-FET sensors can exceed the Nernst limit, (i.e., pH sensitivity of greater than 59.5 mV pH^{-1} at 300 K), by operating the device under dual gate [31] or in a DG configuration [24].

Selectivity of SiNW-FET sensors towards other metal ions can be introduced by modifying the oxide layer of SiNW. For example, Luo et al. reported the use of 3-mercaptopropyltriethoxysilane (MPTES) modified SiNWs for selective detection of Cd^{+2} and Hg^{+2} ions with detection limits of 10^{-4} M and 10^{-7} M, respectively [5]. The selectivity of MPTES modified SiNWs towards Cd^{+2} and Hg^{+2} ions was driven by soft acid (Cd^{+2} and Hg^{+2} ions) and soft base (thiol) interaction, which provided ca. 55% change in the current response. In the presence of hard and intermediately hard acids as based on Mg^{+2}, Ca^{+2}, Ba^{+}, K^{+}, Na^{+}, Cu^{+2}, Co^{+2} and Ni^{+2} ions, the change in current response was less than 3%. The reusability of the SiNW sensor was demonstrated for one cycle by incubating the sensing surface in an acidic solution for 24 h. In another example, Cui et al. modified the surface of SiNW with CaM for selective detection of Ca^{+2} ions [3].

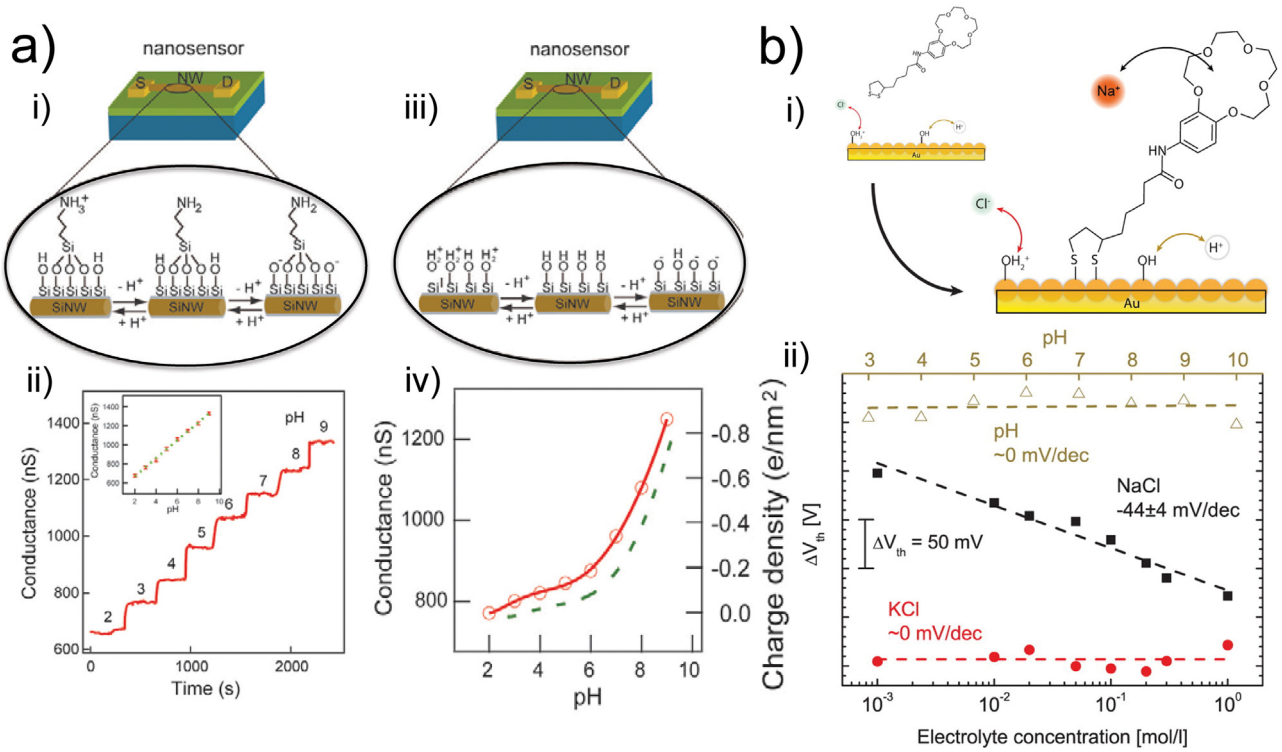

Fig. 11. (a) SiNW-FET sensor for pH measurements. (i) Schematics of an APTES modified SiNW connected by the source and drain electrodes; changes in the surface charge state of an APTES film with pH. (ii) Real-time changes in conductance response of APTES-modified p-type SiNW for pH values of 2–9. (Inset) Conductance vs. pH plot. (iii) Schematics of an unmodified SiNW with surface silanol groups and changes in surface charge state of silanol groups with pH. (iv) Conductance response of an unmodified SiNW as a function of pH (red curve). Changes in surface charge density for silanol groups as a function of pH (green dashed curve). (b) Sodium sensing using Au-coated SiNWs modified with sodium selective crown ethers. (i) Immobilization scheme for the conjugation of sodium-selective crown ether on the surface of Au-coated SiNW. (ii) Differential threshold voltage (ΔV_{th}) response of Au-coated SiNW-FET sensors as function of electrolyte concentration and pH. Note: the response of the NW is only selective for Na^+ ions. Figures in panel (a) reprinted with permission from reference [107]. Figures in panel (b) reprinted with permission from reference [4] (For interpretation of the references to colour in this figure legend, the reader is referred to the web version of this article.).

While the bare SiO_2 layer on the surface of SiNWs has been used for pH sensing [34,104], this surface functionality is inherently limited due to its cross reactivity (ion pairing of surface silanol groups) with other electrolytes, such as NaCl and KCl [105]. This cross reactivity is a function of the ionic strength of the solution and is typically observed under high ionic strength (>10 mM) [105].

The reliability of the response exhibited by SiNW-FET sensors can be improved by implementing a differential measurement as reported by Wipf et al. [4]. In this approach, the response of unmodified NWs served as an internal standard, and the signal was subtracted from the response of active NWs (NW modified with selective chemistry) to account for background interferences. The authors reported the selective detection of Na^+ ions using Au-coated SiNWs that were modified with Na-selective crown ethers as shown in Fig. 11b(i). Despite the presence of selective agent on the surface of Au-coated SiNWs, the NWs exhibited a concentration dependent response in the presence of chloride and hydronium ions. This was attributed to the interaction of chloride and hydronium ions with Au-oxide functional groups that were present on the surface of the Au film. To account for this non-selective interaction, the response of unmodified Au-coated SiNWs was subtracted from the response of active crown ether modified Au-coated SiNWs at the threshold voltage [106]. By incorporating a differential measurement, the Au-coated SiNW-FET sensor only showed a response in the presence of Na^+ ions as shown in Fig. 11b(ii).

3.2. Nucleic acid detection using SiNWs

SiNW-FETs are attractive sensors for label-free detection of nucleic acids. The negative charge associated with the sugar-phosphate backbone of DNA and RNA allows sensitive detection of nucleic acids with detection limits in the fM range [8,53,108]. Even greater relative changes in surface charge can be achieved by using analogs of DNA probes that are electrostatically neutral. For example, PNA [109] and alkylphosphonate oligonucleotide [110] chemistries used in probe construction offer improved signal-to-noise ratio as compared to DNA probes given that the probe is uncharged and hybridization with DNA or RNA introduces a significant change in charge [48,73,81,109]. Probes with electrically neutral backbones offer reduced background conductance signal as compared to DNA probes which are negatively charged [83]. Additionally, a PNA–DNA hybrid is energetically more stable (higher melting temperature) as compared to a DNA–DNA hybrid at the same ionic strength [111], resulting in improved hybridization efficiency as compared to DNA probes at low ionic strength conditions. Low ionic strength conditions are advantageous from the standpoint of enhanced sensitivity from SiNW-FET sensors owing to the increased Debye screening length. Moreover, PNA probes are capable of binding with complementary sequences that are double stranded [112–114]. SiNW-FETs modified with PNA probes have been reported for genotyping associated with cystic fibrosis transmembrane receptor gene [8] and single nucleotide polymorphism (SNP) detection [72]. Applications of SiNW-FETs for nucleic acid detection include implementation of PNA probes, and the use of DNA probes [72,76].

Zhang et al. reported label-free detection of microRNA (miRNA) using an n-type SiNW-FET sensor and PNA as capture probes [109]. The miRNA targets have a length of 18–24 nucleotides. These short strands are known to serve important roles in cellular physiology such as in the regulation of gene expression and in signaling processes that are associated with cancer development [115]. The

change in resistance of SiNWs functionalized with PNA was found to be proportional to the concentration of FC miRNA (Fig. 12a(i)). The resistance of the SiNW increased with increasing concentration of miRNA target, which is an expected response from n-type SiNWs where the hybridization of negatively charged miRNA targets resulted in a decrease in the density of charge carriers inside SiNW. The limit of detection (LOD) of the assay was reported to be 1 fM and the hybridization assays showed no response in the presence of NC miRNA target. SNP detection with a contrast ratio of ca. 5 to 1 was also demonstrated (Fig. 12a(ii)). Hybridization assays conducted with PNA probes provided 5-fold higher assay sensitivity as compared to DNA probes (Fig. 12a(iii)). Similar improvement in the assay sensitivity (4-fold) for a PNA as compared to a DNA modified SiNW-FET sensor was also reported

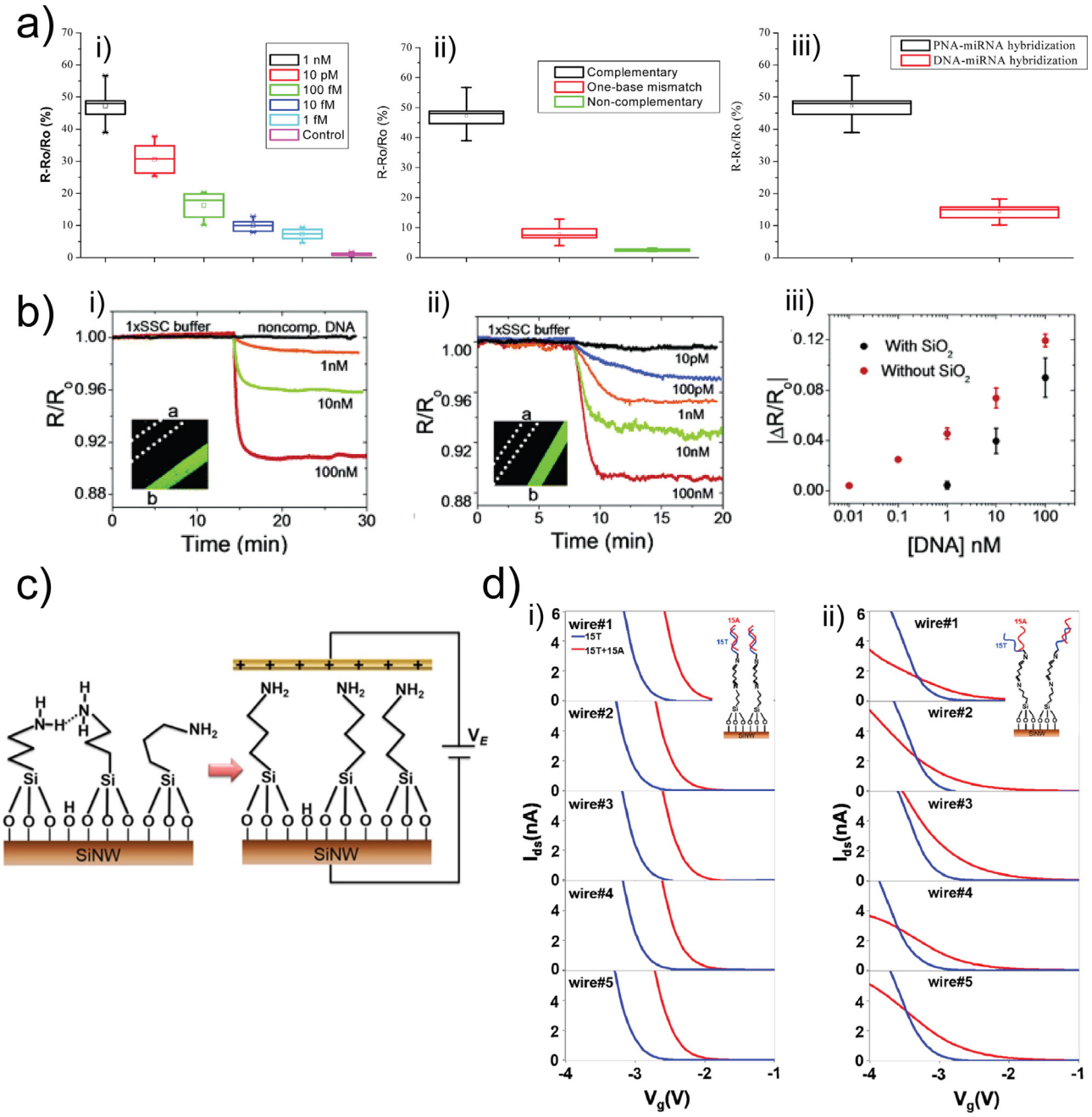

Fig. 12. (a) (i) Relative change in resistivity versus miRNA concentration for PNA-modified n-type SiNW-FET sensor. (ii) Response of the SiNW-FET sensor modified with PNA probes to FC, 1 base pair mismatch (1 BPM) and NC miRNA target at 1 nM concentration each. (iii) Response of the PNA-modified and DNA-modified SiNW-FET sensor to 1 nM concentration of FC miRNA targets. (b) Real-time response of the p-type SiNW-FET sensor in the presence of FC targets that was modified in the (i) presence and (ii) absence of oxide layer with electrostatically adsorbed oligonucleotide probes. Note the difference in the detection limits of (i) and (ii), being 1 nM and 10 pM, respectively. The black traces correspond to the assay response in the presence of NC targets. (Inset) Fluorescence images of microfluidic channels in the presence of labeled (a) NC and (b) FC targets. (iii) Concentration dependent response from SiNWs modified in the presence and absence of the oxide layer. (c) Schematic representation showing electric field mediated alignment of APTES film. (d) Current versus backgate voltage response of SiNW-FET sensor for a nucleic acid hybridization assay (i) with and (ii) without electric field mediated alignment of interfacial chemistry. Blue and red curves represent before and after introduction of target oligonucleotides, respectively. The results shown are for five replicate measurements that were done with different NWs. Figures in panel (a) reprinted with permission from reference [109]. Figures in panel (b) reprinted with permission from reference [76]. Figures in panel (c) and (d) reprinted with permission from reference [108] (For interpretation of the references to colour in this figure legend, the reader is referred to the web version of this article.).

by Li et al. [73]. It should be noted that detection of these small sequences using indirect methods such as fluorescence often necessitates additional processing steps such as polymerase chain reaction and isothermal amplification [116–118], which can potentially bias the concentration levels of these small oligonucleotides in the original sample [109].

Real-time detection of nucleic acid hybridization using SiNW-FET sensors at physiologically relevant conditions (0.165 M) was reported by Bunimovich et al. [76]. To facilitate the positioning of the binding interaction within the Debye screening length (ca. 1 nm for 0.165 M), DNA probes were electrostatically adsorbed onto amine terminated SiNWs. Additionally, in order to improve the sensitivity of the device, the oxide layer was etched prior to surface modification of SiNWs with amine functionality. The authors reported that the SiNWs that were modified with amine functionality in the presence of an oxide layer provided 2 orders of magnitude higher detection limit (1 nM compared with 10 pM) and 2 orders of magnitude lower dynamic range as compared to the SiNWs that were modified with amine functionality after etching of the oxide layer (Fig. 12b). Using time-based measurements, the kinetic and thermodynamic parameters obtained for the hybridization reactions of the SiNW-FET sensors were found to be comparable to those obtained with the surface plasmon resonance sensor. Hybridization experiments with NC targets provided no response from SiNW-FET sensor. However, no data was presented about partial mismatch discrimination. The authors reported that signals for the hybridization of oligonucleotides reached steady state in minutes, which is consistent with diffusion-limited mixing in microfluidic environments [119]. The work by Stern et al. showed that hybridization times within seconds can be achieved by using turbulent flow for sample delivery [78].

The sensitivity of the response exhibited by SiNWs can be dependent on the strength of molecular dipole moments that localize on the surface of SiNWs, which in turn is governed by the degree of alignment and structural ordering of the interfacial chemistry [77]. For example, Lin et al. showed that the "global polarizability" of an APTES film that is covalently attached to the surface of SiNW can be induced by an externally applied backgate voltage (Fig. 12c) [77]. This resulted in a higher conductance response from SiNWs than in the absence of a backgate voltage where molecular dipoles associated with APTES film were randomly oriented. Chu et al. showed that the sensitivity of a nucleic acid hybridization assay conducted with SiNW-FET sensors can be improved by electric field mediated alignment of interfacial chemistry [108]. The alignment of interfacial chemistry was done at each step of the assembly to immobilize single stranded oligonucleotide probes (15 mer) on the surface of SiNWs. As can be seen in Fig. 12d(i), the NWs that were subjected to alignment by electric field exhibited a parallel shift in current versus backgate voltage response upon target hybridization. On the other hand, no such parallel shift was observed for the NWs in the absence of an alignment process (Fig. 12d(ii)). This parallel shift is indicative of a constant dipole field from the interfacial chemistry on the surface of the NWs. A randomly oriented dipole field makes the current response less susceptible to the backgate voltage, hence no parallel shift in the gate voltage is observed [108]. The authors reported a detection limit of 0.1 fM for DNA probe and target sequences that were 15 BP in length [108]. The two factors that were responsible for the improvement in assay sensitivity upon electric field mediated alignment of interfacial chemistry were enhancement of the electric field dipole moment that was generated on the surface of SiNW upon a hybridization reaction, and improvement in the hybridization efficiency.

The size and shape of SiNWs are important aspects that govern the sensitivity of FET sensors [57]. The work by Gao et al. showed that the sensitivity of SiNW-FET sensors can be improved by implementing SiNWs with a triangularly shaped cross section [120]. These were fabricated by the top–down approach using CMOS compatible methods, and allowed for reduction of the diameter of the NWs to 20 nm. The authors reported a LOD of 1 fM for a hybridization assay using oligonucleotide target strands that were 19 BP in length. A multiplexed detection of two nucleic acid targets that were diagnostic for strains of AIV was also described. In a subsequent study, Gao et al. reported a LOD of 0.1 fM for an oligonucleotide target strand that was 24 BP long using triangularly shaped SiNW-FET sensors (Fig. 13a) [53]. The improved LOD was ascribed to the optimization of the assay conditions in terms of the concentration of oligonucleotide probe solution that was deposited (0.5 μM; Fig. 13b), ionic strength of the solution (0.01 × PBS; Fig. 13c) and the application of a backgate voltage in the sub-threshold regime. It should be noted that the detection limit of 0.1 fM is the lowest that has been reported with SiNW-FET sensors for nucleic acid detection. This detection limit is also lower than many other nucleic acid hybridization assays that have been reported using various transducers [121–126]. Further improvement in LOD below 0.1 fM is possible by integration of nucleic acid amplification methods as was recently demonstrated by Gao et al. [127]. The authors reported a LOD of 50 aM for a nucleic acid hybridization assay conducted with SiNW-FET sensors by implementing a rolling circle amplification (RCA) following target hybridization. The integration of RCA resulted in a greater number of negative charges introduced at the SiNW surface. Table 3 provides a list of selected examples of various nucleic acid hybridization assays that have been reported with SiNW-FET sensors. It can be seen that the LOD of various assays is strongly influenced by the design of interfacial chemistry and the hybridization conditions (e.g., ionic strength).

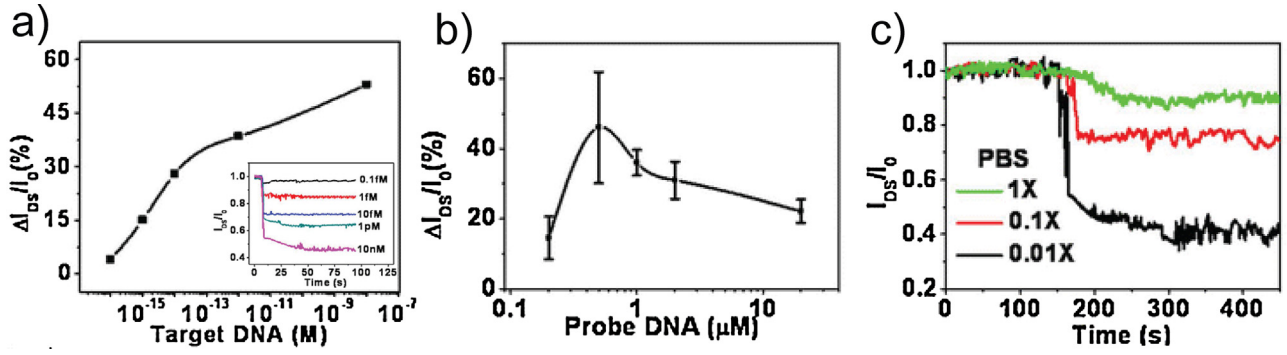

Fig 13. (a) Normalized change in current response of the SiNW-FET sensor modified with DNA probe as a function of target oligonucleotide concentration. (Inset) Time dependent response of the sensor to various target concentrations (0.1 fM, 1 fM, 10 fM, 1 pM and 10 nM). Optimization of the assay response showing normalized change in current as a function of (b) probe concentration (target concentration at 10 nM; ionic strength of the solution at 0.1 × PBS) and (c) ionic strength of the solution (probe concentration at 2 μM; target concentration at 10 nM). Figures reprinted with permission from reference [53].

Table 3
Selected examples of DNA-based SiNW-FET sensors with reported assay conditions, detection limits and target sequence length.

Capture probe (target length)	Limit of detection (LOD)	Buffer composition, ionic strength, Debye screening length	Notes	Reference
DNA (16 BP)	10 pM	1 × SSC, 165 mM *ca.* 1 nm	Electrostatically adsorbed capture probe, oxide layer removed by etching.	[76]
PNA (22 BP)	10 fM	0.01 × SSC, 1.65 mM 7.0 nm	Oxide layer removed by chemical etching and SiNW surface passivated with an organic film.	[81]
PNA (22 BP)	1 fM	0.01 × SSC, 1.65 mM 7.0 nm	Electrostatically neutral analog of DNA as a capture probe.	[109]
DNA (19 BP)	1 fM	0.1 × PBS 15 mM 2.3 nm	Small size of SiNWs achieved by implementation of NW structures with triangular cross section.	[120]
DNA (24 BP)	0.1 fM	0.01 × PBS, 1.5 mM 7.3 nm	Triangularly shaped SiNW-FETs operated at "subthreshold" regime.	[53]
DNA (15 BP)	0.1 fM	0.01 × PBS, 1.5 mM 7.3 nm	Alignment of interfacial chemistry by electric field.	[108]
DNA (30 BP)	50 aM	0.1 × PBS 15 mM 2.3 nm	RCA amplification.	[127]

3.3. Immunodetection using SiNWs

The sensitivity of SiNW-FETs is severely hampered by charge screening effects in complex biological samples such as blood due to the high concentration of electrolyte (>100 mM) and the associated reduction in the Debye screening length. Additionally, the performance of FET sensors in serum samples can degrade due to non-specific adsorption of proteins such as albumin, which constitutes about half of all serum proteins [128]. As a result, detection of biomarkers in serum samples often requires *ex situ* sample treatment steps such as filtering, desalting and buffer exchange prior to detection [129]. The limitations imposed by the Debye screening length on the sensitivity of FET sensors become even more pronounced for immunological detection strategies due to the size of antibodies (≥10 nm). It has been suggested that intact antibodies are impractical to use in conjunction with FET-based detection of antigens under physiological conditions, as the separation distance (10–14 nm) between the sensor surface and charges on an analyte that is bound to a capture antibody is well beyond the Debye length. As a result, most immunoassay studies with SiNW-FETs are done using low ionic strength (1 μM to 1 mM) conditions [17,129]. For example, Huang et al. reported no detectable response from SiNW-FET sensors that were modified with PSA antibody for selective detection of PSA when the assays were conducted in 1× and 0.1 × PBS solutions, λ_D = 0.7 nm and 2.4 nm, respectively [130]. Detectable responses from the FET sensors were observed in 0.01 × PBS solution (λ_D = 7.5 nm). The Debye screening length at this condition surpassed the dimensions of PSA antibody (4.2 nm). However, a potential drawback of this approach is that it lowers the buffer capacity of a solution, making it more susceptible to pH changes upon target analyte introduction. This can also potentially affect the charge state of an analyte. It should be noted that it is the charge state of an analyte that is responsible for field gating the NW conduction channel. Moreover, changing the buffer capacity of a solution has been reported to affect protein function and signal-to-noise ratio response of NW-FETs [131]. Given that the ionic strength of most physiologically relevant samples is ≥100 mM, it would be useful to find ways to overcome the Debye screening length limitation associated with NW-FET devices for immunological detection.

The work by Elnathan et al. showed that it is possible to use the selective binding fragments of antibodies to place biorecognition events within the Debye screening length, thereby greatly improving assay sensitivity within physiologically relevant ionic strength conditions [22]. The authors subjected the capture antibody to two sequential fragmentation steps in order to trim the size of antibody and reduce the distance of the biorecognition event from the surface of a sensor as shown in Fig. 14a(i). In the first step, an intact antibody (size: 9–10 nm) was subjected to Pepsin digestion to form $F(ab)_2$ fragments (size: 4–5 nm). The enzyme Pepsin degrades Fc portion of the heavy chains of an antibody below the interchain disulfide bridges, leaving the two Fab portions of an antibody intact and connected by a disulfide bridge. In the second step, 2-mercaptoethylamine (2-MEA) was used as a reducing agent to cleave the remaining disulfide to liberate two Fab fragments (size: 2–3 nm). The antibodies used in the work targeted cardiac Troponin T (cTnT) and cardiac Troponin I (cTnI) antigens, which serve as biomarkers for diagnosis of acute myocardial infarction. The intact antibody and its fragments were immobilized on the surface of aldehyde modified SiNWs via lysine residues.

Using an intact antibody for cTnI (anti-cTnI), the analytical performance of an enzyme-linked immunosorbent assay (ELISA) was compared with that of a SiNW-FET sensor. The assays were conducted at low ionic strength of 0.1 mM (Debye length = ca. 20 nm). The SiNW-FET sensor provided 6 orders of magnitude lower LOD as compared to the ELISA assay. The LOD of the ELISA assay was 40 pM (1 ng/mL), while the SiNW-FET sensor provided a LOD of 40 aM (1 fg/mL). Experiments conducted with intact anti-cTnT, $F(ab)_2$ and Fab fragments under low ionic strength of 0.1 mM indicated that the fragmentation of antibody resulted in some loss in reactivity (Fig. 14a(ii)). For a constant concentration of cTnT at 40 nM, FETs that were modified with intact anti-cTnT and $F(ab)_2$ and Fab fragments exhibited a sensitivity response of Fab > $F(ab)_2$ > intact anti-cTnT under various ionic strength conditions (Fig. 14a(iii)). For a low ionic strength (0.001 × PBS, 0.15 mM) of solution, the intact anti-cTnT and both of the fragments exhibited the same conductivity response within experimental precision. This was expected due to a large Debye length (ca. 20 nm) under these ionic strength conditions. However, the response from intact anti-cTnT was indistinguishable from the background when the ionic strength was increased to

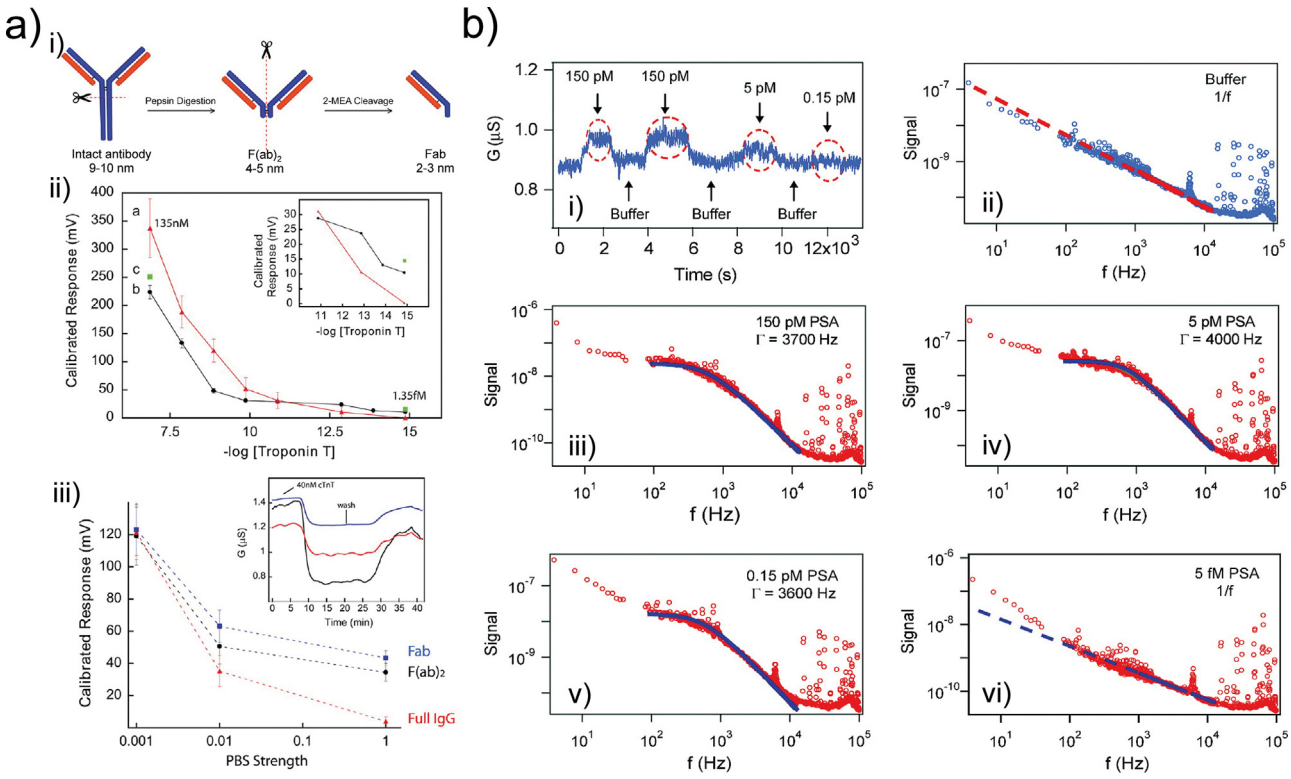

Fig. 14. (a) (i) Schematic of the steps for the generation of $F(ab)_2$ and Fab fragments from an intact antibody by sequential treatments with Pepsin digestion and 2-MEA. (ii) Response of a SiNW-FET sensor modified with intact anti-cTnT (red), $F(ab)_2$ fragment (black) and Fab fragment (green) to different concentrations of cTnT in 0.1 mM ionic strength. The red and green curves are virtually identical. (Inset) An expanded view showing the response of the assay at low concentrations of cTnT. (iii) Response of a SiNW-FET sensor modified with intact IgG (red), $F(ab)_2$ fragments (black) and Fab fragments (blue) under different ionic strength conditions. Note that with increasing ionic strength, the response of Fab fragment > $F(ab)_2$ fragment > intact IgG. (Inset) Real-time response of three different SiNWs modified with $F(ab)_2$ anti-cTnT to 40 nM cTnT in 1 × PBS. (b) (i) Time domain conductance response and (ii–vi) frequency domain conductance response of SiNW-FET sensor modified with anti-PSA to (ii) 0 nM (buffer), (iii) 150 pM, (iv) 5 pM, (v) 0.15 pM and (vi) 5 fM concentrations of PSA. In the time domain, the NW response to 0.15 pM of PSA is indistinguishable from the background, while in the frequency domain, the exposure of 0.15 pM of PSA still exhibits a Lorentzian shape. The NW responses in (ii) and (vi) are identical and show $1/f$ frequency dependence. The experimental data in (ii–vi) are shown as circles while the fits are shown as lines. Panel (a) reprinted with permission from reference [22] and panel (b) reprinted with permission from reference [136] (For interpretation of the references to colour in this figure legend, the reader is referred to the web version of this article.).

1 × PBS (150 mM, Debye length ca. 0.7 nm), and only $F(ab)_2$ and Fab fragments showed conductivity changes above the background. The authors also investigated the selective detection of cTnT in undiluted serum samples using SiNW-FETs modified with anti-cTnT $F(ab)_2$ fragment, and reported a LOD of 27 pM. Additionally, it was also reported that the density of surface coverage with antibody plays an important role in determining the sensitivity of FET device. Optimum response was observed with an intact anti-cTnT immobilization density of 1.8×10^{11} molecules cm^{-2}.

An alternative to use of fragments of capture antibodies is the implementation of antibody mimic proteins (AMPs) as selective agents for immunodetection as was reported by Ishikawa et al. using NW-FET sensors [132]. AMPs are polypeptides that range in size from 2 to 5 nm and have high binding affinity for target analyte (dissociation constant in nM range) [133]. AMPs are developed by *in vitro* selection methods and can be engineered to retain their activity over a range of ionic strength and pH conditions [134]. AMPs can potentially improve the sensitivity of FET sensors by: (1) allowing the binding interaction to take place within the Debye screening length at higher ionic strengths; (2) allowing assays to be conducted at a pH condition at which the surface charge on the analyte is maximized [21]; (3) allowing optimization of the dissociation constant for a particular ionic strength (cf. loss of antigen-antibody interaction for PSA was observed for low ionic strength of a 0.001 × PBS solution [130]); and (4) providing for control of the attachment of AMPs to the surface of NWs via introduction of functional groups (such as sulfhydryl groups or azides) in locations that are distant from the selective binding site.

Use of a selective binding interactions where a relatively small antigen-like molecule is immobilized was reported by Hideshima et al. [135]. The authors compared the analytical performance of SiNW-FET sensors that were modified with two different capture agents, sialic acid containing oligosaccharide (size: ca. 2 nm) and antibody (size: 4–14 nm), for selective detection of hemagglutinins associated with human and avian influenza virus. Assays conducted with oligosaccharide modified FETs provided 6 orders of magnitude lower LOD (50 aM) as compared to the assays con-ducted with the antibody (50 pM). Owing to the small size of the oligosaccharide as compared to the antibody, the assay sensitivity was improved by allowing a greater proportion of analyte charge to remain within the vicinity of Debye screening length.

Zheng et al. reported that electrical measurements made in the frequency domain can improve the LOD of SiNW-FET sensors as shown in Fig. 14b [136]. In the frequency (f) domain, the power spectrum of the voltage noise for a current-biased SiNW-FET sensor exhibits $1/f$ dependence due to a combination of thermal fluctuations, and fluctuations in the density and mobility of charge carriers [127]. In the presence of a selective interaction that has reached equilibrium, the fluctuations in the SiNW-FET signal can be modeled as a combination of a Lorentzian fit with a characteristic frequency (Γ), that is superimposed on the characteristic $1/f$ background noise spectrum. No correlation between the characteristic frequency and the concentration of target analyte (PSA) was found. However, the signal associated with 0.15 pM of PSA was distinguishable from the background in the frequency domain (Fig. 14b(v)). At the same

operating conditions the time domain measurements (Fig. 14b(i)) showed no signal above the background. The frequency domain signal offered 30 fold lower LOD (0.15 pM) and 10 fold improvement in assay sensitivity as compared to conventional time domain conductance signal (LOD of 5 pM) based on the separation of $1/f$ background noise from the Lorentzian frequency.

3.3.1. Multiplexed detection

Multiplexed detection of biomarkers is important for accurate diagnosis of complex diseases such as cancer [137]. It has been reported that concurrent detection of 3 to 5 biomarkers is typically required to establish reliable diagnosis [138]. Zheng et al. reported the label-free, real-time and multiplexed detection of the three cancer biomarkers, PSA-α1-antichymotrypsin (PSAα1), carcinoembryonic antigen (CEA) and mucin-1, with fM sensitivity in undiluted serum samples [75]. In order to achieve multiplexing, a device consisting of integrated SiNW arrays was developed in which different regions of the SiNW arrays (p-type or/and n-type) were modified with different mAbs. The sample delivery was done using a microfluidic channel made of a PDMS cover that was bonded to the device chip (Fig. 15a).

Experiments conducted with SiNWs that were modified with PSAα1-specific mAb showed that the conductance change was proportional to the concentration of PSAα1 from 5 ng/mL to 90 fg/mL (Fig. 15b). Real-time data showed that the conductance increased and then returned to the base-line upon alternate introduction of PSAα1 and buffer solutions into a microfluidic channel, indicating that the binding was reversible. The LODs of PSAα1, CEA and mucin-1 were found to be 75 fg/mL (2 fM), 100 fg/mL (0.55 fM) and 75 fg/mL (0.49 fM), respectively. The contribution of non-specific adsorption was evaluated by simultaneous and sequential introduction of PSAα1 and BSA solutions at 0.9 pg/mL and 10 μg/mL respectively, to a device in which NWs were modified with a mAb that was selective for PSAα1. The introduction of various mixtures of PSAα1 and BSA in solution showed responses that only corresponded to the concentration of PSAα1, suggesting that the presence of BSA did not interfere with the selective binding of PSA. No change in conductance was observed when BSA solution was injected into a microfluidic channel, suggesting the absence of significant non-specific interactions (Fig. 15c).

Multiplexed detection of three cancer biomarkers, PSAα1, CEA and mucin-1, was demonstrated using SiNW arrays modified with mAbs for PSAα1 (NW1), CEA (NW2) and mucin-1 (NW3). The conductance versus time response was recorded from each of the different modified NWs, and solutions containing PSAα1, CEA or mucin-1 were sequentially introduced into the microfluidic chip. The conductance changes recorded from each NW were only observed in the presence of the relevant target biomarker in the sample solution, and the changes were proportional to the concentration of the corresponding biomarker (Fig. 15d). SiNWs that were not modified with mAbs, and p-type and n-type NWs modified with the same capture mAbs were also incorporated into the device to account for any contributions to the signals due to non-specific adsorption.

Zhang et al. also reported a multiplexed detection of three cardiac biomarkers: cTnT, creatine kinase MM (CK-MM) and creatine kinase MB (CK-MB) [139]. Samples were from a 2 μL fingerprick blood volume, and were interrogated using a SiNW-FET sensor array. The analysis was completed in 45 min using an

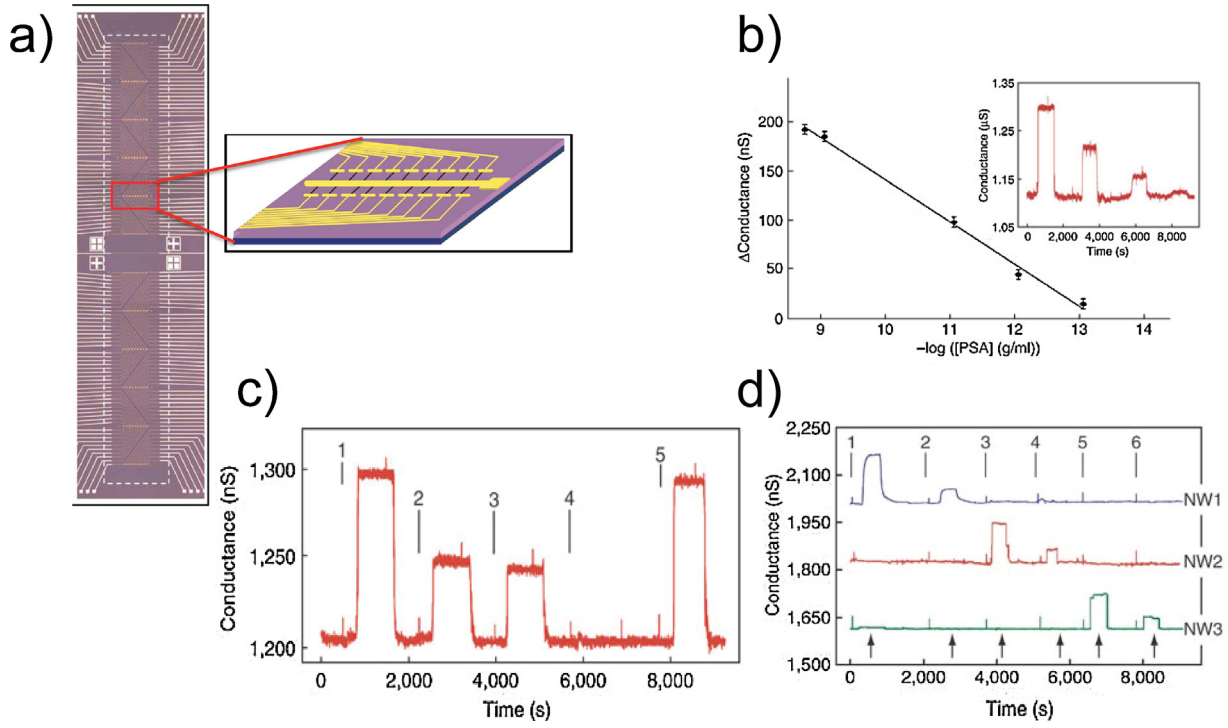

Fig. 15. (a) Optical image of the SiNW-FET sensors for a multiplexed detection of three cancer biomarkers. White lines represent metal electrodes connected to individual SiNW devices. The white dashed rectangular box represents the chip area that was covered by a microfluidic channel. The arrangement of the source and drain electrodes in the horizontal red rectangle is shown in the zoomed in image. (b) Concentration dependent change in conductance of SiNW modified with PSAα1-mAb to increasing concentration of PSAα1. (Inset) Time dependent change in conductance to alternating delivery of PSAα1 and buffer solutions with decreasing concentration of PSAα1. PSAα1 concentrations were 0.9 ng/mL, 9 pg/mL, 0.9 pg/mL and 90 fg/mL with increasing time. (c) Conductance versus time data recorded for SiNWs that were modified with PSAα1-mAb for alternating delivery of protein and buffer solutions. (1) 9 pg/mL PSAα1, (2) 0.9 pg/mL PSAα1, (3) 0.9 pg/mL PSAα1 and 10 μg/mL BSA, (4) 10 μg/mL BSA and (5) 9 pg/mL PSAα1. (d) Conductance versus time data for simultaneous detection of PSAα1, CEA and mucin-1 in which NW1, NW2 and NW3 were modified with mAbs for PSAα1, CEA and mucin-1, respectively. The solutions were sequentially delivered inside a microfluidic channel. (1) 0.9 ng/mL PSAα1, (2) 1.4 pg/mL PSAα1, (3) 0.2 ng/mL CEA, (4) 2 pg/mL CEA, (5) 0.5 ng/mL mucin-1 and (6) 5 pg/mL mucin-1. After the injection of each protein sample solution, buffer solution was injected into the channel at points indicated by black arrows. Figure reprinted with permission from reference [75].

integrated chip that consisted of a filtration assembly for separation of plasma from blood and a SiNW-FET array for detection. Filtration was mechanical, and used submicron (<0.8 μm) vertical pillar gap microstructures to allow only plasma from blood to pass through. The fluid was subsequently delivered to the SiNW-FET array for detection. Multiplexing was achieved by spatial registration where different regions of the SiNW-FET sensor array were functionalized with different mAbs for the detection of the targeted proteins with a LOD of 1 pg mL^{-1}. Zhang et al. subsequently published another study that described multiplexed detection of cTnT, CK-MM and CK-MB in serum samples with a LOD of 100 fg mL^{-1} using SiNW-FETs [140]. For this second study, no sample processing involving dilution of serum samples or filtration of plasma from blood was required before detection. Additionally, the readout was done using an application specific integrated circuit (ASIC). This approach offered concurrent electrical measurements from multiple SiNWs at a frame rate of kilo-samples per second. In the previous study, the readout was done using a probe station analyzer that suffered from low throughput as it required a minute for one sensor measurement.

3.4. Cellular investigations using SiNW-FET probes

Interfacing nanomaterials with cells provides an opportunity to probe and manipulate biological processes occurring inside cells. The diameter (1–100 nm) of SiNWs is much smaller than the typical diameter of cells (ca. 10 μm). SiNWs can enable cellular recordings with high spatial (μm) and temporal resolution (sub-millisecond), and also support multiplexed detection [13,14,141]. Moreover, the high aspect ratio of NWs is advantageous from the standpoint of supporting mechanical deformation of NWs for enhanced interfacial coupling with cells [142,143]. This observation is consistent with reports that interfaces that are based on nanomaterials can facilitate and influence adhesion of cells [144].

Numerous studies have reported the integration of SiNW-FET sensors to probe electrophysiology associated with single cells [12,59], tissues [14] and intact organs [15,59] in a spatiotemporal manner owing to the ultra-high sensitivity and fast detection capabilities of SiNW sensors. For example, Patolsky et al. reported that an array of SiNW-FETs that was supported on a planar substrate can be used to stimulate action potential and monitor the rate of electrical signal propagation associated with individual neurons and dendrites [12]. Additionally, bottom–up synthesized SiNWs have also been integrated with flexible and transparent polymeric substrates to allow for simultaneous optical imaging and electrical measurements [15]. The flexible nature of these substrates allows deformation, which provides for increased interfacial interaction at the cell/NW or tissue/NW interface, while also potentially facilitating integration of these devices for *in vivo* studies. It has been reported that the cell/SiNW interface can affect the sensitivity [13] and spatial resolution [14] of the electrical measurements.

While planar nanoscale FET devices have shown great potential for high-resolution extracellular electrical measurements and for *in vitro* sensing applications [145], the planar configuration of these devices limits their use for intracellular detection owing to the close proximity of source and drain electrodes with the NW [146]. Additionally, SiNW-FETs that are supported on planar

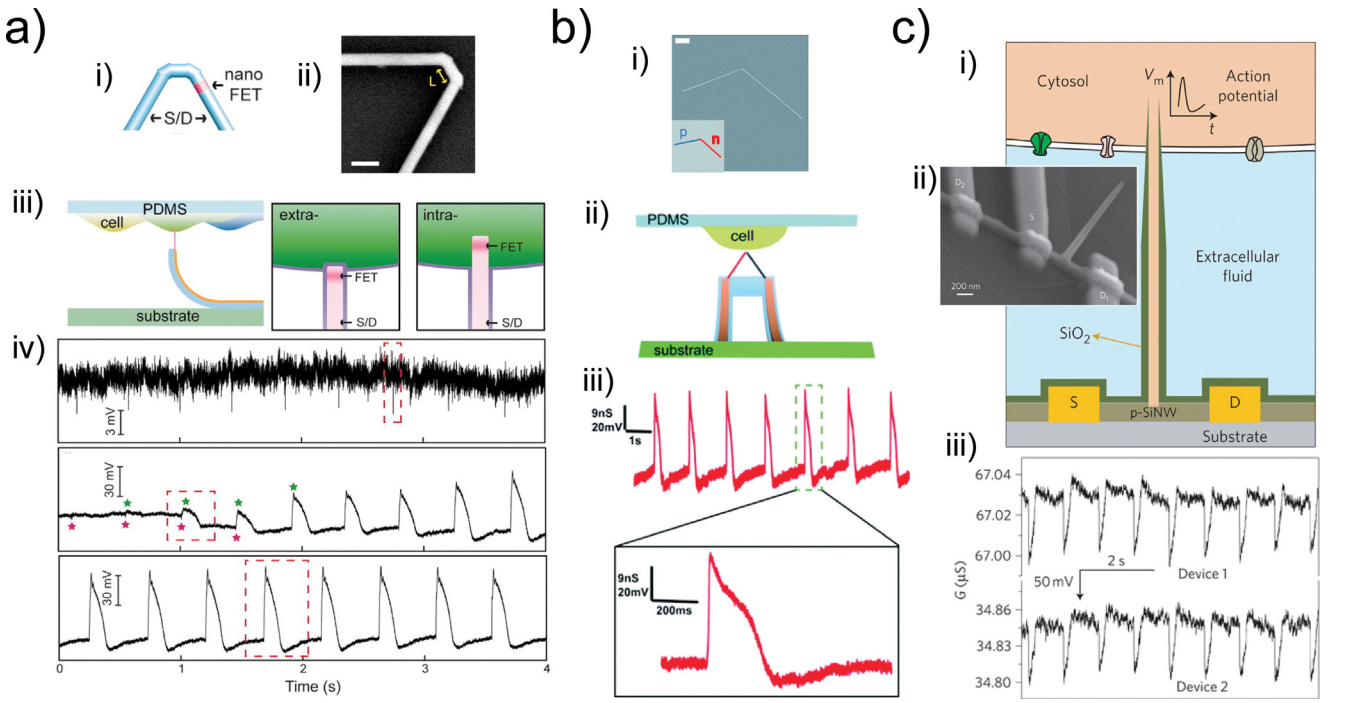

Fig. 16. Intracellular recording of electrical signals associated with spontaneously firing cardiomyocyte cells using (a) doubly-kinked SiNW-FET with cis configuration, (b) single-kinked pn junction SiNW nanoprobe and (c) BIT-FET. (a) (i) Schematic of a doubly-kinked SiNW with source and drain arms sandwiching a nano-FET. (ii) SEM image of a doubly-kinked SiNW. The scale bar represents 200 nm. (iii) Schematic of a set-up for electrical recordings from a monolayer of cardiomyocyte cells that were cultured on a slab of PDMS and lipid coated doubly-kinked SiNW-FET that was placed at an angle with respect to the supporting substrate for the cell/NW interface (left). Extracellular (middle) and intracellular (right) cell/NW interfaces. (iv) Transition of electrical recordings during cell entrance from extracellular (top) to intracellular (middle) and stable intracellular recording (bottom). (b) (i) SEM image of a single-kinked pn junction SiNW nanoprobe. (ii) Schematic of a set-up for intracellular electrical recordings from cardiomyocyte cells that were cultured as a monolayer on a PDMS slab using pn junction SiNW nanoprobe. (iii) (Top) Steady-state intracellular electrical recordings from cardiomyocyte cells. (Bottom) Expanded profile of the single action potential associated with the dashed green rectangle. (c) (i) Schematic of the association of BIT-FET with the cytosol (orange) of individual cell. The S and D electrodes (in yellow) surround each side of the SiO_2 nanotube (shown in green). The extracellular medium is shown in light blue. (ii) SEM image of a FET device (left) without and (right) with SiO_2 nanotube. (iii) Intracellular electrical recordings from a single cardiomyocyte cell using two BIT-FET devices. Panel (a) reprinted with permission from reference [147]. Panel (b) reprinted with permission from reference [11]. Panel (c) reprinted with permission from reference [10] (For interpretation of the references to colour in this figure legend, the reader is referred to the web version of this article.).

substrates are physically limited in providing adequate interfacial coupling with cells and tissues for high sensitivity electrical measurements. To address this limitation, Tian et al. reported the development of doubly kinked SiNWs with cis configuration, where the tip of each kinked SiNW harbored a nanoscale FET as shown in Fig. 16a(i) [147]. Interfacing of the doubly kinked SiNW-FETs with embryonic chicken cardiomyocytes cells for intracellular electrical measurements required that the kinked SiNWs were coated with a phospholipid bilayer using 1,2-dimyristoyl-sn-glycero-3-phosphocholine (DMPC) to facilitate cell membrane fusion (Fig. 16a(iii) and (iv)) [147]. A key aspect to recording intracellular action potential was the flexible nature of the support (patterned poly(methylmethacrylate) and Su-8 microribbins) onto which the doubly kicked SiNWs were supported, as intracellular electrical measurements were only possible when the kinked NW was oriented at an angle greater than 50° with respect to the planar substrate [147]. Similarly, single-kinked SiNWs that were coated with DMPC have been integrated with spontaneously firing cardiomyocyte cells for high resolution intracellular recording of action potentials in a spatiotemporal manner (Fig. 16b) [11]. Overall, kinked FET probes facilitate intracellular association and detection by placing the source and drain electrodes away from the active sensor area which is typically localized at the tip of a kinked SiNW. The spatial resolution that can be achieved with these kinked NWs is limited owing to the size of these probes (ca. 200 nm). To address this limitation, Duan et al. reported the development of branched intracellular nanotube FET (BIT-FET) that consisted of a SiNW-FET detector that was oriented orthogonally to a hollow SiO_2 nanotube as shown in Fig. 16c(i) [10]. The BIT-FET with a tip size of 55 nm (tip outer diameter) was used for

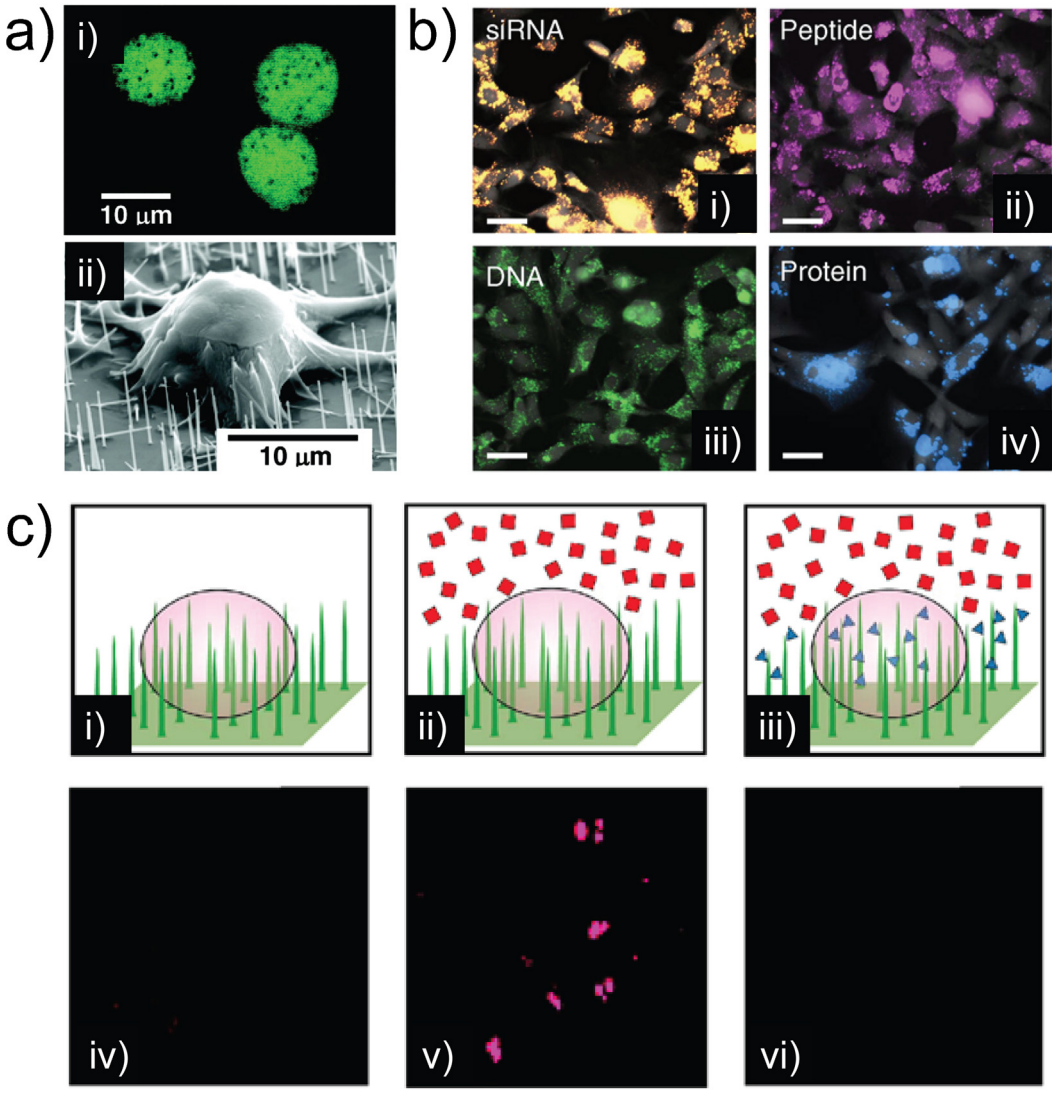

Fig. 17. Vertically aligned SiNWs as a platform for intracellular delivery of molecules. (a) (i) Confocal microscopy image and (ii) SEM image showing penetration of mouse embryonic stem (mES) cells by vertically aligned array of SiNWs. In (i), the SiNWs appear as black dots in the vicinity of mES cells that were expressing green fluorescent protein. (b) Epi-fluorescence images showing transfection of human fibroblasts with fluorescently labeled (i) siRNA, (ii) peptides, (iii) plasmid DNA and (iv) proteins using vertically aligned SiNW platform. (c) Schematics of apoptosis inhibition using vertically aligned SiNWs that were modified with apoptosis inhibition peptide for intracellular delivery. HeLa cells cultured in the (i) absence and (ii) presence of apoptosis-inducing agents, actinomycin-D (Act-D) and tumor necrosis factor-alpha (TNF-α), shown as red squares. In (iii) the cells were also cultured in the presence of Act-D and TNF-α except the NWs were modified with apoptosis-inhibiting peptide (blue triangles). The results of the terminal deoxynucleotidyl transferase dUTP nick end labeling (TUNEL) assay corresponding to conditions (i), (ii) and (iii) are shown in (iv), (v) and (vi), respectively. It can be seen that the culture of HeLa cells in the presence of vertical SiNWs that were modified with apoptosis-inhibition peptide showed no evidence of exposed nuclei (absence of pink stain). The negative control in (iv) and the positive control in (v) showed the expected absence and presence of exposed nuclei, respectively. Panel (a) reprinted with permission from reference [148], and panels (b) and (c) reprinted with permission from reference [149] (For interpretation of the references to colour in this figure legend, the reader is referred to the web version of this article.).

intracellular recordings of full action potential associated with the spontaneously firing of embryonic chicken cardiomyocytes in a multiplexed format (Fig. 16c(iii)). The small tip size was speculated to be advantageous to support lipid fusion and to form a tight seal upon intracellular penetration. Additionally, the small internal volume (ca. 3 aL) associated with the nanotube is useful to promote cell viability.

3.4.1. Intracellular delivery of agents

It has been reported that an array of vertical SiNWs not only supports mammalian cell culture, but also provides direct physical access to the intracellular environment by penetrating cells without affecting the electrophysiology of the cultured cells (Fig. 17a) [19,148]. This offers an intriguing method that might find use in the introduction of analytical reagents and nanoparticle bioprobes to living cells. Kim et al. reported that the survival of the cultured cells is a function of the SiNW diameter, where the survival of the cultured cells improved as the diameter of the SiNWs was reduced from 400 nm to 30 nm, offering a survival of less than a day to greater than 5 days, respectively [148]. The authors also reported that SiNWs with electrostatically adsorbed plasmid DNA could be used as a platform to transfect cells with genetic material (plasmid DNA expressing green fluorescence protein). In another study by Shalek et al., the authors reported that a diverse array of molecules that included small molecules, small interfering RNA (siRNA), protein, peptide and DNA can be individually and concurrently introduced inside various cell types using vertically aligned SiNWs with greater than 95% transfection efficiency (Fig. 17b) [149]. The molecules were electrostatically adsorbed onto SiNWs that were modified with APTMS. The authors reported that the phenotypic expression of various cell types can be perturbed by delivery of various effector molecules inside cells, where the delivery of effector molecules that were adsorbed on the surface of SiNWs was mediated by penetration of SiNWs inside cells (e.g., apoptosis inhibition in Fig. 17c). Overall, these studies are useful as they provide the design criteria that can potentially facilitate the integration of SiNW-FET probes for intracellular detection of biochemical events.

4. Summary and conclusions

Sensors based on SiNW-FETs are attractive as they offer direct, label-free, real-time and sensitive detection of target analytes with detection limits in fM range (for biomolecule detection such as proteins and nucleic acids). Nanoscale FETs offer improved sensitivity as compared to planar FET devices as a result of the nanometer dimensions which increase the surface area to volume ratio. Methods have been developed for synthesis of single-crystal SiNWs where the selection and concentration of dopant can be varied to tune electrical properties. Moreover, surface modification of SiNWs for receptor immobilization is facilitated by well-established methods of silane chemistry.

The analytical performance of SiNW-FET sensors is governed by many factors. These factors can be broadly categorized into: (1) solution-phase assay conditions; (2) interfacial chemistry for selective binding; and (3) the physical structure, assembly and operation of devices. Learning to control these factors will be important from the standpoint of improving the reliability of measurements that are made using SiNW-FET sensors. The confidence in measurements that are made using SiNW-FET devices can be improved by incorporating multiple copies of NWs to validate the results from a statistical perspective. Additionally, NW sensors that operate as internal references can be integrated into a device to account for signal variations associated with device fabrication. NWs with opposite dopant types (p-type and n-type) functionalized with the same selective chemistry can also be integrated into a single sensor chip, which will result in opposing conductivity response change upon analyte binding. Variations in the signal strength from the two types of device elements can then be used to account for signal variation imposed by device fabrication.

In the area of nucleic acid detection, none of the studies that have been reported with SiNWs have shown regeneration of the selective interface. It has been suggested that the use of harsh acidic or basic conditions can degrade the contact lines on the device, while use of high temperatures can change the electrical properties of NWs [109]. Other methods are available to achieve regeneration which avoid the use of high temperatures and harsh conditions, such as denaturation of hybrids using chaotropes (e.g., formamide) and modulation of stringency by ionic strength manipulation [123]. While these devices can potentially offer large multiplexing capability, there are numerous challenges that are hindering progress. Methods are needed to spatially place, register and selectively functionalize each NW-FET sensor with a selective agent to achieve multiplexing. Alignment methods based on electric fields can control the orientation and number of NWs bridging the source and drain electrodes. However, these methods do not provide spatial registration, which is a necessity for multiplexed detection using these devices. It has been shown that it is possible to functionalize NWs with PNA probes prior to alignment and integration of NW sensors on a device. It is yet not clear if the same methodology can be applied to antibodies as they are more susceptible to denaturation, especially when subjected to photolithographic methods for NW integration.

The size of a SiNW-FET probe and flexibility of a substrate material are paramount in governing the intracellular integration, cellular viability, resolution and sensitivity of the measurements that are made using SiNW-FET sensors. Many of these requirements have been met by advances in the bottom–up synthesis of SiNWs that have allowed for *in situ* control of morphology, orientation, dopant types and concentration of dopants during the synthesis of SiNWs. However, to date majority of these studies have focused on electrical recordings from cells and tissues in a spatiotemporal manner. Additionally, vertically aligned SiNWs have been shown to passively penetrate cells, providing a means to transfect cells with a variety of agents. It will be interesting to see if SiNW-FETs can be used to probe dynamic biochemical events that constitute various cellular functions such as gene expression levels and events associated with signal cascade inside cells.

Acknowledgements

The authors gratefully acknowledge the Natural Sciences and Engineering Research Council of Canada (NSERC) for financial support of this research. M.O.N is also grateful to the Ontario Ministry of Training, Colleges and Universities (MTCU) for provision of an Ontario Graduate Scholarship (OGS).

References

[1] D.A. Giljohann, C.A. Mirkin, Nature 462 (2009) 461–464.
[2] F.P. Zamborini, L.L. Bao, R. Dasari, Analytical Chemistry 84 (2012) 541–576.
[3] Y. Cui, Q.Q. Wei, H.K. Park, C.M. Lieber, Science 293 (2001) 1289–1292.
[4] M. Wipf, R.L. Stoop, A. Tarasov, K. Bedner, W. Fu, I.A. Wright, C.J. Martin, E.C. Constable, M. Calame, C. Schönenberger, ACS Nano 7 (2013) 5978–5983.
[5] L.B. Luo, J.S. Jie, W.F. Zhang, Z.B. He, J.X. Wang, G.D. Yuan, W.J. Zhang, L.C.M. Wu, S.T. Lee, Applied Physics Letters 94 (2009).
[6] M.C. McAlpine, H.D. Agnew, R.D. Rohde, M. Blanco, H. Ahmad, A.D. Stuparu, W.A. Goddard, J.R. Heath, Journal of the American Chemical Society 130 (2008) 9583–9589.
[7] W.U. Wang, C. Chen, K.H. Lin, Y. Fang, C.M. Lieber, Proceedings of the National Academy of Sciences of the United States of America 102 (2005) 3208–3212.
[8] J. Hahm, C.M. Lieber, Nano Letters 4 (2004) 51–54.
[9] A. Kim, C.S. Ah, H.Y. Yu, J.H. Yang, I.B. Baek, C.G. Ahn, C.W. Park, M.S. Jun, S. Lee, Applied Physics Letters 91 (2007).

[10] X.J. Duan, R.X. Gao, P. Xie, T. Cohen-Karni, Q. Qing, H.S. Choe, B.Z. Tian, X.C. Jiang, C.M. Lieber, Nature Nanotechnology 7 (2012) 174–179.
[11] Z. Jiang, Q. Qing, P. Xie, R.X. Gao, C.M. Lieber, Nano Letters 12 (2012) 1711–1716.
[12] F. Patolsky, B.P. Timko, G.H. Yu, Y. Fang, A.B. Greytak, G.F. Zheng, C.M. Lieber, Science 313 (2006) 1100–1104.
[13] T. Cohen-Karni, B.P. Timko, L.E. Weiss, C.M. Lieber, Proceedings of the National Academy of Sciences of the United States of America 106 (2009) 7309–7313.
[14] Q. Qing, S.K. Pal, B.Z. Tian, X.J. Duan, B.P. Timko, T. Cohen-Karni, V.N. Murthy, C.M. Lieber, Proceedings of the National Academy of Sciences of the United States of America 107 (2010) 1882–1887.
[15] B.P. Timko, T. Cohen-Karni, G.H. Yu, Q. Qing, B.Z. Tian, C.M. Lieber, Nano Letters 9 (2009) 914–918.
[16] J.Y. Yu, S.W. Chung, J.R. Heath, The Journal of Physical Chemistry B 104 (2000) 11864–11870.
[17] F. Patolsky, G.F. Zheng, O. Hayden, M. Lakadamyali, X.W. Zhuang, C.M. Lieber, Proceedings of the National Academy of Sciences of the United States of America 101 (2004) 14017–14022.
[18] B.Z. Tian, P. Xie, T.J. Kempa, D.C. Bell, C.M. Lieber, Nature Nanotechnology 4 (2009) 824–829.
[19] J.T. Robinson, M. Jorgolli, A.K. Shalek, M.H. Yoon, R.S. Gertner, H. Park, Nature Nanotechnology 7 (2012) 180–184.
[20] X. Duan, Y. Li, N.K. Rajan, D.A. Routenberg, Y. Modis, M.A. Reed, Nature Nanotechnology 7 (2012) 401–407.
[21] E. Stern, J.F. Klemic, D.A. Routenberg, P.N. Wyrembak, D.B. Turner-Evans, A.D. Hamilton, D.A. LaVan, T.M. Fahmy, M.A. Reed, Nature 445 (2007) 519–522.
[22] R. Elnathan, M. Kwiat, A. Pevzner, Y. Engel, L. Burstein, A. Khatchtourints, A. Lichtenstein, R. Kantaev, F. Patolsky, Nano Letters 12 (2012) 5245–5254.
[23] A. Poghossian, A. Cherstvy, S. Ingebrandt, A. Offenhausser, M.J. Schoning, Sensors and Actuators B 111 (2005) 470–480.
[24] J.H. Ahn, J.Y. Kim, M.L. Seol, D.J. Baek, Z. Guo, C.H. Kim, S.J. Choi, Y.K. Choi, Applied Physics Letters 102 (2013).
[25] F. Patolsky, G.F. Zheng, C.M. Lieber, Analytical Chemistry 78 (2006) 4260–4269.
[26] Y.F. Zhang, Y.H. Tang, N. Wang, D.P. Yu, C.S. Lee, I. Bello, S.T. Lee, Applied Physics Letters 72 (1998) 1835–1837.
[27] Y. Cui, X.F. Duan, J.T. Hu, C.M. Lieber, The Journal of Physical Chemistry B 104 (2000) 5213–5216.
[28] J.T. Hu, T.W. Odom, C.M. Lieber, Accounts of Chemical Research 32 (1999) 435–445.
[29] N. Elfstrom, A.E. Karlstrom, J. Linnrost, Nano Letters 8 (2008) 945–949.
[30] N. Elfstrom, J. Linnros, Nanotechnology 19 (2008).
[31] O. Knopfmacher, A. Tarasov, W.Y. Fu, M. Wipf, B. Niesen, M. Calame, C. Schonenberger, Nano Letters 10 (2010) 2268–2274.
[32] S. Rosenblatt, Y. Yaish, J. Park, J. Gore, V. Sazonova, P.L. McEuen, Nano Letters 2 (2002) 869–872.
[33] X.P.A. Gao, G.F. Zheng, C.M. Lieber, Nano Letters 10 (2010) 547–552.
[34] S.Y. Chen, J.G. Bomer, E.T. Carlen, A. van den Berg, Nano Letters 11 (2011) 2334–2341.
[35] J. Go, P.R. Nair, B. Reddy, B. Dorvel, R. Bashir, M.A. Alam, ACS Nano 6 (2012) 5972–5979.
[36] J.H. Ahn, S.J. Choi, J.W. Han, T.J. Park, S.Y. Lee, Y.K. Choi, Nano Letters 10 (2010) 2934–2938.
[37] A.K. Wanekaya, W. Chen, N.V. Myung, A. Mulchandani, Electroanalysis 18 (2006) 533–550.
[38] K.-I. Chen, B.-R. Li, Y.-T. Chen, Nano Today 6 (2011) 131–154.
[39] R.M. Penner, Annual Reviews in Analytical Chemistry 5 (2012) 461–485.
[40] B. Reddy, B.R. Dorvel, J. Go, P.R. Nair, O.H. Elibol, G.M. Credo, J.S. Daniels, E.K.C. Chow, X. Su, M. Varma, M.A. Alam, R. Bashir, Biomedical Microdevices 13 (2011) 335–344.
[41] B.R. Dorvel, B. Reddy, J. Go, C.D. Guevara, E. Salm, M.A. Alam, R. Bashir, ACS Nano 6 (2012) 6150–6164.
[42] R.G. Hobbs, N. Petkov, J.D. Holmes, Chemistry of Materials 24 (2012) 1975–1991.
[43] M. Law, J. Goldberger, P.D. Yang, Annual Reviews of Materials Research 34 (2004) 83–122.
[44] W. Lu, C.M. Lieber, Journal of Physics D: Applied Physics 39 (2006) R387–R406.
[45] V. Schmidt, J.V. Wittemann, U. Gosele, Chemical Reviews 110 (2010) 361–388.
[46] V. Schmidt, J.V. Wittemann, S. Senz, U. Gosele, Advanced Materials 21 (2009) 2681–2702.
[47] J. Ramanujam, D. Shiri, A. Verma, Materials Express 1 (2011) 105–126.
[48] Z.Q. Gao, A. Agarwal, A.D. Trigg, N. Singh, C. Fang, C.H. Tung, Y. Fan, K.D. Buddharaju, J.M. Kong, Analytical Chemistry 79 (2007) 3291–3297.
[49] J.L. Liu, Y. Lu, Y. Shi, S.L. Gu, R.L. Jiang, F. Wang, Y.D. Zheng, Applied Physics A: Materials Science & Processing 66 (1998) 539–541.
[50] Y. Wu, Y. Cui, L. Huynh, C.J. Barrelet, D.C. Bell, C.M. Lieber, Nano Letters 4 (2004) 433–436.
[51] A.M. Morales, C.M. Lieber, Science 279 (1998) 208–211.
[52] M.N. Masood, S. Chen, E.T. Carlen, A. van den Berg, ACS Applied Materials & Interfaces 2 (2010) 3422–3428.
[53] A.R. Gao, N. Lu, Y.C. Wang, P.F. Dai, T. Li, X.L. Gao, Y.L. Wang, C.H. Fan, Nano Letters 12 (2012) 5262–5268.
[54] Y.L. Bunimovich, G. Ge, K.C. Beverly, R.S. Ries, L. Hood, J.R. Heath, Langmuir 20 (2004) 10630–10638.
[55] C.R. Leao, A. Fazzio, A.J.R. da Silva, Nano Letters 7 (2007) 1172–1177.
[56] Y. Cui, L.J. Lauhon, M.S. Gudiksen, J.F. Wang, C.M. Lieber, Applied Physics Letters 78 (2001) 2214–2216.
[57] N. Elfstrom, R. Juhasz, I. Sychugov, T. Engfeldt, A.E. Karlstrom, J. Linnros, Nano Letters 7 (2007) 2608–2612.
[58] A. Javey, S. Nam, R.S. Friedman, H. Yan, C.M. Lieber, Nano Letters 7 (2007) 773–777.
[59] T.S. Pui, A. Agarwal, F. Ye, N. Balasubramanian, P. Chen, Small 5 (2009) 208–212.
[60] R.S. Wagner, W.C. Ellis, Applied Physics Letters 4 (1964) 89–90.
[61] B. He, T.J. Morrow, C.D. Keating, Current Opinion in Chemical Biology 12 (2008) 522–528.
[62] D. Whang, S. Jin, Y. Wu, C.M. Lieber, Nano Letters 3 (2003) 1255–1259.
[63] G.H. Yu, A.Y. Cao, C.M. Lieber, Nature Nanotechnology 2 (2007) 372–377.
[64] Y. Huang, X.F. Duan, Q.Q. Wei, C.M. Lieber, Science 291 (2001) 630–633.
[65] E.M. Freer, O. Grachev, X.F. Duan, S. Martin, D.P. Stumbo, Nature Nanotechnology 5 (2010) 525–530.
[66] M.W. Li, R.B. Bhiladvala, T.J. Morrow, J.A. Sioss, K.K. Lew, J.M. Redwing, C.D. Keating, T.S. Mayer, Nature Nanotechnology 3 (2008) 88–92.
[67] Z.Y. Fan, J.C. Ho, Z.A. Jacobson, R. Yerushalmi, R.L. Alley, H. Razavi, A. Javey, Nano Letters 8 (2008) 20–25.
[68] Y.-K. Chang, F.C.-N. Hong, Nanotechnology 20 (2009).
[69] J.W. Durham, Y. Zhu, ACS Applied Materials & Interfaces 5 (2013) 256–261.
[70] F. Xu, J.W. Durham, B.J. Wiley, Y. Zhu, ACS Nano 5 (2011) 1556–1563.
[71] P.L. Chiang, T.C. Chou, T.H. Wu, C.C. Li, C.D. Liao, J.Y. Lin, M.H. Tsai, C.C. Tsai, C.J. Sun, C.H. Wang, J.M. Fang, Y.T. Chen, Chemistry – An Asian Journal 7 (2012) 2073–2079.
[72] Z. Li, Y. Chen, X. Li, T.I. Kamins, K. Nauka, R.S. Williams, Nano Letters 4 (2004) 245–247.
[73] Z. Li, B. Rajendran, T.I. Kamins, X. Li, Y. Chen, R.S. Williams, Applied Physics A: Materials Science & Processing 80 (2005) 1257–1263.
[74] Y.C.C. Liu, N. Rieben, L. Iversen, B.S. Sorensen, J. Park, J. Nygard, K.L. Martinez, Nanotechnology 21 (2010) 245105–245111.
[75] G.F. Zheng, F. Patolsky, Y. Cui, W.U. Wang, C.M. Lieber, Nature Biotechnology 23 (2005) 1294–1301.
[76] Y.L. Bunimovich, Y.S. Shin, W.-S. Yeo, M. Amori, G. Kwong, J.R. Heath, Journal of the American Chemical Society 128 (2006) 16323–16331.
[77] M.C. Lin, C.J. Chu, L.C. Tsai, H.Y. Lin, C.S. Wu, Y.P. Wu, Y.N. Wu, D.B. Shieh, Y.W. Su, C.D. Chen, Nano Letters 7 (2007) 3656–3661.
[78] E. Stern, R. Wagner, F.J. Sigworth, R. Breaker, T.M. Fahmy, M.A. Reed, Nano Letters 7 (2007) 3405–3409.
[79] B. Dorvel, B. Reddy, R. Bashir, Analytical Chemistry 85 (2013) 9493–9500.
[80] S.H. Park, U. Krull, Analytica Chimica Acta 564 (2006) 133–140.
[81] G.-J. Zhang, J.H. Chua, R.-E. Chee, A. Agarwal, S.M. Wong, K.D. Buddharaju, N. Balasubramanian, Biosensors and Bioelectronics 23 (2008) 1701–1707.
[82] W.J. Royea, A. Juang, N.S. Lewis, Applied Physics Letters 77 (2000) 1988–1990.
[83] G.-J. Zhang, G. Zhang, J.H. Chua, R.-E. Chee, E.H. Wong, A. Agarwal, K.D. Buddharaju, N. Singh, Z. Gao, N. Balasubramanian, Nano Letters 8 (2008) 1066–1070.
[84] B.R. Li, C.W. Chen, W.L. Yang, T.Y. Lin, C.Y. Pan, Y.T. Chen, Biosensors and Bioelectronics 45 (2013) 252–259.
[85] H. Haick, P.T. Hurley, A.I. Hochbaum, P. Yang, N.S. Lewis, Journal of the American Chemical Society 128 (2006) 8990–8991.
[86] C.J. Barrelet, D.B. Robinson, J. Cheng, T.P. Hunt, C.F. Quate, C.E.D. Chidsey, Langmuir 17 (2001) 3460–3465.
[87] M.M. Sung, G.J. Kluth, O.W. Yauw, R. Maboudian, Langmuir 13 (1997) 6164–6168.
[88] A. Bansal, N.S. Lewis, The Journal of Physical Chemistry B 102 (1998) 4058–4060.
[89] A. Bansal, N.S. Lewis, The Journal of Physical Chemistry B 102 (1998) 1067–1070.
[90] L.J. Webb, N.S. Lewis, The Journal of Physical Chemistry B 107 (2003) 5404–5412.
[91] I. Park, Z.Y. Li, A.P. Pisano, R.S. Williams, Nano Letters 7 (2007) 3106–3111.
[92] F.H. Arnold, Nature Biotechnology 9 (1991) 151–156.
[93] J. Schmitt, H. Hess, H.G. Stunnenberg, Molecular Biology Reports 18 (1993) 223–230.
[94] Y.S. Lo, D.H. Nam, H.M. So, H. Chang, J.J. Kim, Y.H. Kim, J.O. Lee, ACS Nano 3 (2009) 3649–3655.
[95] T. Cha, A. Guo, X.Y. Zhu, Proteomics 5 (2005) 416–419.
[96] K. Bonroy, F. Frederix, G. Reekmans, E. Dewolf, R. De Palma, G. Borghs, P. Declerck, B. Goddeeris, Journal of Immunological Methods 312 (2006) 167–181.
[97] S.P. Lin, C.Y. Pan, K.C. Tseng, M.C. Lin, C.D. Chen, C.C. Tsai, S.H. Yu, Y.C. Sun, T.W. Lin, Y.T. Chen, Nano Today 4 (2009) 235–243.
[98] T.W. Lin, P.J. Hsieh, C.L. Lin, Y.Y. Fang, J.X. Yang, C.C. Tsai, P.L. Chiang, C.Y. Pan, Y. T. Chen, Proceedings of the National Academy of Sciences of the United States of America 107 (2010) 1047–1052.
[99] T.Y. Lin, B.R. Li, S.T. Tsai, C.W. Chen, C.H. Chen, Y.T. Chen, C.Y. Pan, Lab on a Chip 13 (2013) 676–684.
[100] M. Nishida, S. Harada, S. Noguchi, Y. Satow, H. Inoue, K. Takahashi, Journal of Molecular Biology 281 (1998) 135–147.
[101] X.X. Duan, N.K. Rajan, D.A. Routenberg, J. Huskens, M.A. Reed, ACS Nano 7 (2013) 4014–4021.
[102] J. Li, Y. Zhang, S. To, L. You, Y. Sun, ACS Nano 5 (2011) 6661–6668.
[103] Y. Chen, X.H. Wang, M. Hong, S. Erramilli, P. Mohanty, Sensors and Actuators B 133 (2008) 593–598.

[104] I. Park, Z. Li, A.P. Pisano, R.S. Williams, Nanotechnology 21 (2010).
[105] A. Tarasov, M. Wipf, R.L. Stoop, K. Bedner, W.Y. Fu, V.A. Guzenko, O. Knopfmacher, M. Calame, C. Schonenberger, ACS Nano 6 (2012) 9291–9298.
[106] H. Ron, I. Rubinstein, Langmuir 10 (1994) 4566–4573.
[107] F. Patolsky, C.M. Lieber, Materials Today 8 (2005) 20–28.
[108] C.J. Chu, C.S. Yeh, C.K. Liao, L.C. Tsai, C.M. Huang, H.Y. Lin, J.J. Shyue, Y.T. Chen, C.D. Chen, Nano Letters 13 (2013) 2564–2569.
[109] G.J. Zhang, J.H. Chua, R.E. Chee, A. Agarwal, S.M. Wong, Biosensors and Bioelectronics 24 (2009) 2504–2508.
[110] W.Y. Chen, H.C. Chen, Y.S. Yang, C.J. Huang, H.W.H. Chan, W.P. Hu, Biosensors and Bioelectronics 41 (2013) 795–801.
[111] H. Park, A. Germini, S. Sforza, R. Corradini, R. Marchelli, W. Knoll, Biointerphases 2 (2007) 80–88.
[112] K.K. Jensen, H. Orum, P.E. Nielsen, B. Norden, Biochemistry 36 (1997) 5072–5077.
[113] P.E. Nielsen, M. Egholm, R.H. Berg, O. Buchardt, Science 254 (1991) 1497–1500.
[114] J. Wang, E. Palecek, P.E. Nielsen, G. Rivas, X.H. Cai, H. Shiraishi, N. Dontha, D.B. Luo, P.A.M. Farias, Journal of the American Chemical Society 118 (1996) 7667–7670.
[115] M. Lagos-Quintana, R. Rauhut, W. Lendeckel, T. Tuschl, Science 294 (2001) 853–858.
[116] Y.Q. Liu, M. Zhang, B.C. Yin, B.C. Ye, Analytical Chemistry 84 (2012) 5165–5169.
[117] C.K. Raymond, B.S. Roberts, P. Garrett-Engele, L.P. Lim, J.M. Johnson, RNA 11 (2005) 1737–1744.
[118] Y.Q. Wen, Y. Xu, X.H. Mao, Y.L. Wei, H.Y. Song, N. Chen, Q. Huang, C.H. Fan, D. Li, Analytical Chemistry 84 (2012) 7664–7669.
[119] G.M. Whitesides, Nature 442 (2006) 368–373.
[120] A.R. Gao, N. Lu, P.F. Dai, T. Li, H. Pei, X.L. Gao, Y.B. Gong, Y.L. Wang, C.H. Fan, Nano Letters 11 (2011) 3974–3978.
[121] S.J. Park, T.A. Taton, C.A. Mirkin, Science 295 (2002) 1503–1506.
[122] J.A. Hansen, R. Mukhopadhyay, J.O. Hansen, K.V. Gothelf, Journal of the American Chemical Society 128 (2006) 3860–3861.
[123] M.O. Noor, A. Shahmuradyan, U.J. Krull, Analytical Chemistry 85 (2013) 1860–1867.
[124] S.J. He, B. Song, D. Li, C.F. Zhu, W.P. Qi, Y.Q. Wen, L.H. Wang, S.P. Song, H.P. Fang, C.H. Fan, Advanced Functional Materials 20 (2010) 453–459.
[125] S.K. Rastogi, C.M. Gibson, J.R. Branen, D.E. Aston, A.L. Branen, P.J. Hrdlicka, Chemical Communications 48 (2012) 7714–7716.
[126] X. Mao, Y.Q. Ma, A.G. Zhang, L.R. Zhang, L.W. Zeng, G.D. Liu, Analytical Chemistry 81 (2009) 1660–1668.
[127] A. Gao, N. Zou, P. Dai, N. Lu, T. Li, Y. Wang, J. Zhao, H. Mao, Nano Letters 13 (2013) 4123–4130.
[128] N.L. Anderson, N.G. Anderson, Molecular and Cellular Proteomics 1 (2002) 845–867.
[129] E. Stern, A. Vacic, N.K. Rajan, J.M. Criscione, J. Park, B.R. Ilic, D.J. Mooney, M.A. Reed, T.M. Fahmy, Nature Nanotechnology 5 (2010) 138–142.
[130] Y.W. Huang, C.S. Wu, C.K. Chuang, S.T. Pang, T.M. Pan, Y.S. Yang, F.H. Ko, Analytical Chemistry 85 (2013) 7912–7918.
[131] N. Lloret, R.S. Frederiksen, T.C. Moller, N.I. Rieben, S. Upadhyay, L. De Vico, J.H. Jensen, J. Nygard, K.L. Martinez, Nanotechnology 24 (2013) 035501.
[132] F.N. Ishikawa, H.K. Chang, M. Curreli, H.I. Liao, C.A. Olson, P.C. Chen, R. Zhang, R.W. Roberts, R. Sun, R.J. Cote, M.E. Thompson, C. Zhou, ACS Nano 3 (2009) 1219–1224.
[133] H.K. Binz, P. Amstutz, A. Plückthun, Nature Biotechnology 23 (2005) 1257–1268.
[134] H.K. Binz, A. Plückthun, Current Opinion in Biotechnology 16 (2005) 459–469.
[135] S. Hideshima, H. Hinou, D. Ebihara, R. Sato, S. Kuroiwa, T. Nakanishi, S.I. Nishimura, T. Osaka, Analytical Chemistry 85 (2013) 5641–5644.
[136] G. Zheng, X.P.A. Gao, C.M. Lieber, Nano Letters 10 (2010) 3179–3183.
[137] J.D. Wulfkuhle, L.A. Liotta, E.F. Petricoin, Nature Reviews. Cancer 3 (2003) 267–275.
[138] N. Rifai, M.A. Gillette, S.A. Carr, Nature Biotechnology 24 (2006) 971–983.
[139] G.J. Zhang, Z.H.H. Luo, M.J. Huang, J.J. Ang, T.G. Kang, H.M. Ji, Biosensors and Bioelectronics 28 (2011) 459–463.
[140] G.J. Zhang, K.T.C. Chai, H.Z.H. Luo, J.M. Huang, I.G.K. Tay, A.E.J. Lim, M. Je, Biosensors and Bioelectronics 35 (2012) 218–223.
[141] P.D. Yang, R.X. Yan, M. Fardy, Nano Letters 10 (2010) 1529–1536.
[142] S.J. Pearton, T. Lele, Y. Tseng, F. Ren, Trends in Biotechnology 25 (2007) 481–482.
[143] R.X. Yan, J.H. Park, Y. Choi, C.J. Heo, S.M. Yang, L.P. Lee, P.D. Yang, Nature Nanotechnology 7 (2012) 191–196.
[144] H.E. Jeong, I. Kim, P. Karam, H.J. Choi, P.D. Yang, Nano Letters 13 (2013) 2864–2869.
[145] T. Cohen-Karni, Q. Qing, Q. Li, Y. Fang, C.M. Lieber, Nano Letters 10 (2010) 1098–1102.
[146] W. Lu, C.M. Lieber, Nature Materials 6 (2007) 841–850.
[147] B.Z. Tian, T. Cohen-Karni, Q. Qing, X.J. Duan, P. Xie, C.M. Lieber, Science 329 (2010) 830–834.
[148] W. Kim, J.K. Ng, M.E. Kunitake, B.R. Conklin, P.D. Yang, Journal of the American Chemical Society 129 (2007) 7228–7229.
[149] A.K. Shalek, J.T. Robinson, E.S. Karp, J.S. Lee, D.R. Ahn, M.H. Yoon, A. Sutton, M. Jorgolli, R.S. Gertner, T.S. Gujral, G. MacBeath, E.G. Yang, H. Park, Proceedings of the National Academy of Sciences of the United States of America 107 (2010) 1870–1875.